Orbital Insolation Variations, Intrinsic Climate Variability, and Quaternary Glaciations

Keno Riechers[1,2], Takahito Mitsui[2,3], Niklas Boers[2,3,4], and Michael Ghil[5,6]

[1]Department of Mathematics and Computer Science, Freie Universität Berlin, Berlin, Germany
[2]Potsdam Institute for Climate Impact Research, Potsdam, Germany
[3]Earth System Modelling, School of Engineering & Design, Technical University of Munich, Munich, Germany
[4]Department of Mathematics and Global Systems Institute, University of Exeter, Exeter, UK
[5]Geosciences Department and Laboratoire de Météorologie Dynamique (CNRS and IPSL), Ecole Normale Supérieure and PSL University, Paris, France
[6]Department of Atmospheric and Oceanic Science, University of California at Los Angeles, Los Angeles, United States

Correspondence: Keno Riechers (riechers@pik-potsdam.de)

Abstract. The relative role of external forcing and of intrinsic variability is a key question of climate variability in general and of our planet's paleoclimatic past in particular. Over the last 100 years since Milankovitch's contributions, the importance of orbital forcing has been well established for the last 2.6 Myr and their Quaternary glaciation cycles. A convincing case has also been made for the role of several internal mechanisms that are active on time scales both shorter and longer than the orbital ones. Such mechanisms clearly have a causal role in Dansgaard-Oeschger and Heinrich events, as well as in the mid-Pleistocene transition. We introduce herein a unified framework for the understanding of the orbital forcing's effects on the climate system's internal variability on time scales from thousands to millions of years. This framework relies on the fairly recent theory of nonautonomous and random dynamical systems and it has been successfully applied so far in the climate sciences for problems like the El Niño-Southern Oscillation, the oceans' wind-driven circulation, and other problems on interannual to interdecadal time scales. Finally, we provide further examples of climate applications and present preliminary results of interest for the Quaternary glaciation cycles in general and the mid-Pleistocene transition in particular.

1 INTRODUCTION AND MOTIVATION

In the early 20th century, Milutin Milankovitch presented his theory of ice ages (Milankovitch, 1920). Based on his own calculations and on insightful suggestions from Wladimir Köppen and Alfred Wegener (Imbrie and Imbrie, 1986), he proposed that the transitions between glacial and interglacial climate conditions were primarily caused by variations of incoming solar radiation, which by that time was known to vary in a quasi-periodic manner on slow time scales of tens to hundreds of thousands of years (Poincaré, 1892–1899). These variations of insolation, which arise as a consequence of the gravitational interaction of the Earth with the other planets and with its own Moon, are typically referred to as orbital forcing.

The orbital forcing comprises variations in (i) the eccentricity of the Earth's orbit around the sun with dominant spectral peaks around 400 kyr and 100 kyr; (ii) the obliquity, or axial tilt, i.e., the angle between the Earth's rotational and its orbital

axis, with dominant periodicity around 41 kyr; and (iii) the climatic precession, which determines the phase of the summer solstice along the Earth's orbit and has its most pronounced spectral power around 23 kyr and 19 kyr (Berger, 1978).

For two centuries or so of modern geology, records of our planet's physical and biological past were merely discrete sequences of strata with specific properties, like coloration and composition (Imbrie and Imbrie, 1986). This state of affairs led, after the initial success of the Milankovitch (1920) theory of the ice ages, to severe criticism of the temporal mismatch between insolation minima and glaciation maxima (e.g., Flint, 1971).

The advent of marine-sediment cores after World War II led, for the first time, to the availability of records that were, more or less, continuous in time. Like all climate records, these cores covered limited time intervals and did so with limited resolution and with inaccuracies in absolute dating, as well as in the quantities being measured. Moreover, they posed the problem of inverting proxy records of isotopic and microbiotic counts to physical quantities like temperature and precipitation.

In spite of these limitations, the spectral analysis of deep-sea records allowed Hays et al. (1976) to overcome the difficulties previously encountered by the orbital theory of Quaternary glaciations, in particular the absence of the imprint of precesional and obliquity peaks in glaciation proxy records. Specifically, Hays et al. (1976) were able to create a composite record — back to over 400 kyr b2k, i.e., over 400 000 yr before the year 2000 CE — from two relatively long marine-sediment records of the best quality available in the early 1970s. The authors demonstrated therewith that significant precessional and obliquity peaks near 20 kyr and 40 kyr were present in this record's spectral analysis; see Fig. 1. The power spectrum in the figure also made it quite clear that these peaks were superimposed on a continuous background — the stippled area in the figure — whose total variance much exceeded the sum of the variances present in the peaks.

The work of Hays et al. (1976) and of the subsequent CLIMAP and SPECMAP projects resulted in a much more detailed spatio-temporal mapping of the Quaternary and extended the belief in the pacemaking role of orbital variations into the more remote past. The spectral peaks near 20 kyr and 40 kyr have been widely interpreted within the geological community as evidence for a linear response of the climate system to the orbital forcing (Imbrie and Imbrie, 1986). A third spectral peak at 100 kyr was, however, the most pronounced, but much more difficult to reconcile with the orbital theory of Quarternary glaciations. Since no sufficiently pronounced counterpart can be found in the spectra of the seasonal insolation forcing, Hays et al. (1976) hypothesized a nonlinear response of the climate system in order to explain this dominant periodicity of the late-Pleistocene glacial–interglacial cycles. At the same time, the advent of higher-resolution marine cores and, especially, ice cores from both Greenland and the Antarctica, led to the discovery of Heinrich events (Heinrich, 1988), Dansgaard-Oeschger (D-O) events (e.g., Dansgaard et al., 1993), and Bond cycles (Bond et al., 1997), which were hard to explain by orbital forcing, given their shorter time scales.

In fact, interest in past climates was heightened not only by these striking observational discoveries, but also by the growing concerns about humanity's impact on the climate (SMIC, 1971; National Research Council, 1975). Given the declining temperatures between the 1940s and 1970s — on the one hand, as shown in Fig. 2[1] — and the substantial advances in the description of the Quaternary glaciations, on the other, that interest was mainly in the planet's falling into another ice age (e.g., National Research Council, 1975).
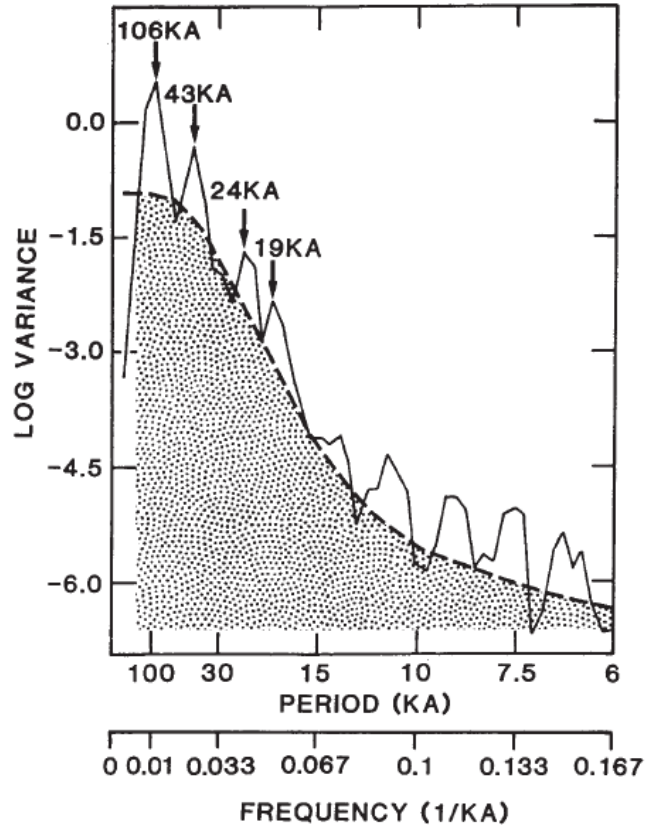
---

[1]see also Ghil and Vautard (1991, Fig. 3)

Figure 1. Power spectrum of a composite $\delta^{18}O$ record using deep-sea cores RC11-120 and E49-18. This figure is based on the work of Hays et al. (1976), as presented by ~~Imbrie and Imbrie (1986)~~Imbrie and Imbrie (1986). ~~From Ghil and Childress (1987) with~~ Reprinted by permission from Springer Nature Customer Service Centre GmbH: Springer Nature. Topics in Geophysical Fluid Dynamics: Atmospheric Dynamics, Dynamo Theory, and Climate Dynamics by Ghil and Childress;©1987 by Springer Science+Business Media New York. All rights reserved. (1987).

55 　As a result of the twofold stimulation provided by data about past glaciations and concern about future ones, a number of researchers in the early-to-mid 1970s worked on energy balance models (EBMs) of climate with multiple stable steady states (Held and Suarez, 1974; North, 1975; Ghil, 1976). Two such stable "equilibria" corresponded to the present climate and to a "deep-freeze," as it was called at the time, i.e., to a totally ice-covered Earth. At the time there was some disbelief about this second climate, as its temperatures were much lower than those associated with the Quaternary glaciations and incompatible
60 with paleoclimatic evidence available in the 1970s.

　New geochemical evidence, though, led in the early 1990s to the discovery of a snowball or, at least, slushball Earth prior to the emergence of multicellular life, sometime before 650 Myr b2k (Hoffman et al., 1998). It thus turned out that this climate state — predicted by several EBMs, and confirmed by a general circulation model (GCM) with much higher spatial resolution (Wetherald and Manabe, 1975) — had actually occurred and it is now being modeled in much greater detail (Pierrehumbert,
65 2004; Ghil and Lucarini, 2020).

　On the other hand, it also became clear that ~~a model~~ these early models, whose only stable solutions were stationary, could not reproduce very well the wealth of variability that the proxy records were describing, not even in the presence of stochastic forcing (e.g., Ghil, 1994). Certain theoretical paleoclimatologists turned, therefore, to coupling a "climate" equation, with
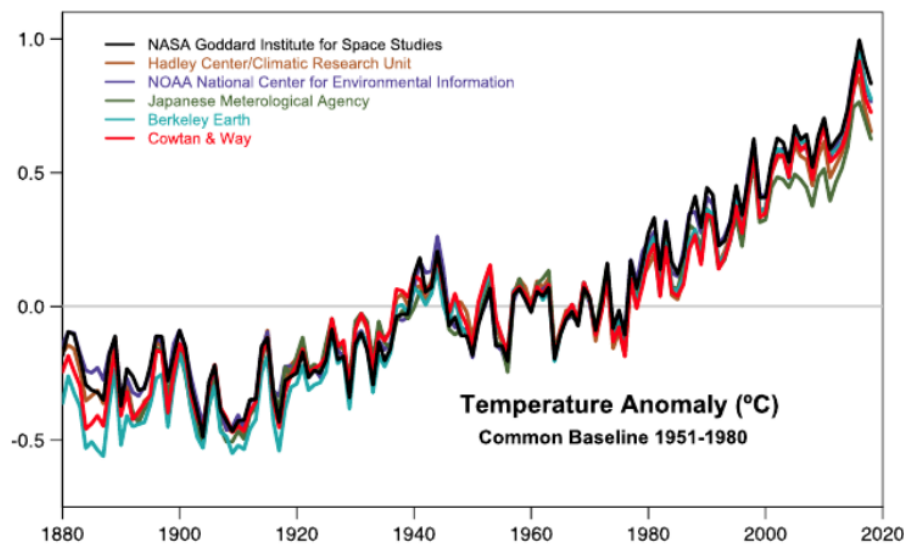

Figure 2. Comparison of six analyses of the annually and globally averaged surface temperature anomalies through 2018. NASA = National Aeronautics and Space Administration; NOAA = National Oceanic and Atmospheric Administration. ~~Reproduced from Lenssen et al. (2019, Fig. 1) with~~ Reprinted by permission from John Wiley & Sons Inc.: American Geophysical Union. Journal of Geophysical Research: Atmospheres. Improvements in the GISTEMP Uncertainty Model. Lenssen et al.;©2019. American Geophysical Union. All Rights Reserved.(2019)

temperature as its only dependent variable, with an ice-sheet equation (Källén et al., 1979; Ghil and Le Treut, 1981) or a
70 carbon-dioxide equation (Saltzman et al., 1981; Saltzman and Maasch, 1988).

These coupled climate models, albeit highly idealized, did produce oscillatory solutions that captured some of the features of the Quaternary glaciation cycles as known at that time. For instance, the models of Ghil and associates (Källén et al., 1979; Ghil and Le Treut, 1981) captured the phase differences between peak ice sheet extent and minimum temperatures ~~suggested by Ruddiman and McIntyre (1981)~~ in the North Atlantic suggested by Ruddiman and McIntyre (1981), while the
75 work of Saltzman and associates (e.g., Saltzman and Maasch, 1988) captured the asymmetry of the glaciation cycles with their more rapid "terminations" (Broecker and Van Donk, 1970).

The stable self-sustained oscillations of these coupled models, though, were totally independent of any orbital or other time-dependent forcing, i.e. the solar input to their radiative budget was constant in time. Hence, they could not capture the wealth of spectral features, with their orbital and other peaks, of the paleorecords available by the 1980s. The basic quandary of the
80 Quaternary glaciation cycles — at least from the point of view of theoretical climate dynamics (Ghil and Childress, 1987, Part IV) — is formulated in Fig. 3 below; see also Ghil (1994)~~.~~: How does the quasi-periodic orbital forcing, with its relatively narrow spectral peaks, act on the climate's internal variability to produce a response that is characterized by significant spectral peaks superimposed on a broad continuous background? And, in particular, how does the climate's spectral peak at 100 kyr arise, given its absence in the power spectrum of the forcing?

85 In this paper, we try to show a path toward resolving the four fundamental questions listed in ~~the box below~~**Box 1**. In the next section, we summarize existing results on how the climate system~~'~~'s intrinsic variability arises ~~at~~ on Quaternary time scales, and on how this variability ~~interacts with~~ is modified by the time-dependent orbital forcing~~. In section~~, which was added to the previously autonomous climate models as the next step in paleoclimate modeling evolution; see, for instance, Le Treut and Ghil (1983) and Le Treut et al. (1988) vs. Ghil and Le Treut (1981). In Sect. 3, we outline a more general frame-
90 work for the study of such ~~interactions~~mechanisms, as given by the theory of nonautonomous and random dynamical systems (NDSs and RDSs), and sketch an application of this theory to other climate problems. An application to the problem at hand is proposed in ~~See~~Sect. 4 and conclusions follow in ~~See~~Sect. 5.

2 SELF-SUSTAINED CLIMATE OSCILLATORS

2.1 A Simple Mechanism for Climate Oscillations

95 We follow Ghil (1994) in sketching the simplest physical mechanism for a self-sustained climate oscillation at fixed insolation forcing. Consider the Källén et al. (1979, KCG hereafter) oscillator, the first such self-sustained climate oscillator, to the best of our knowledge. The model itself was built from the ground up, coupling a scalar version of the ~~Ghil (1976)~~ Ghil (1976) energy balance model (EBM) with a simplified, scalar version of the ~~Weertman (1964, 1976)~~ Weertman (1964, 1976) ice sheet model (ISM). The model's details and further analyses of its ingredients and variants can be found in several references (e.g.,
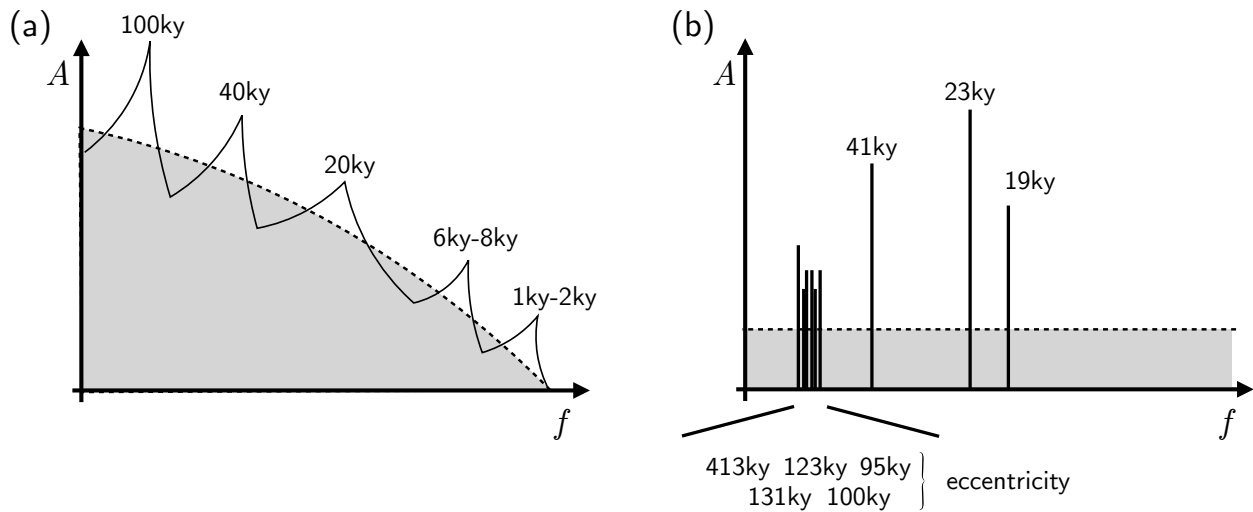100 Crafoord and Källén, 1978; Ghil and Tavantzis, 1983; Ghil, 1984; Bódai et al., 2015).

Figure 3. The theoretical quandary of modeling the Quaternary glaciation cycles, illustrated here by schematic diagrams of the composite power spectra of (a) the paleorecords and (b) the orbital forcing. In panel (a), the dominant peak for the Late Pleistocene is near 100 kyr, while in panel (b) eccentricity forcing is distributed over several spectral lines. The peaks at 6–8 kyr and 1–2 kyr in panel (a) correspond to Bond cycles (Bond et al., 1992, 1993) and to the mean recurrence of D-O events and they lack a match in the forcing lines of panel (b).Courtesy of N. Boers.

> Based on the discussion so far and on the discrepancy between panels (a) and (b) of Fig. 3, we propose herein the following questions that need to be resolved, still, for a thorough understanding of Quaternary climate variability:
>
> 1. How does the dominant peak of the observed variability near 100 kyr arise, given the rather diffuse orbital forcing at this periodicity?
>
> 2. What causes the continuous part of the observed spectrum, which contains most of the variance?
>
> 3. What gives rise to the high-frequency peaks due to the sudden warmings and to the approximate periodicities associated with Heinrich and D-O events, among others?
>
> 4. What are the contributions of the orbital forcing and of the climate system's intrinsic variability to items (1)–(3) and how does the former one modify the latter?

Box 1. Fundamental questions regarding the Quaternary glacial-interglacial glacial–interglacial cycles.

The basic workings of this climate oscillator can be represented by two coupled ordinary differential equations (ODEs), written symbolically as

$$\dot{T} \simeq -V, \tag{1a}$$

$$\dot{V} \simeq T. \tag{1b}$$

Here T stands for global temperature and V for global ice volume, while Eq. (1a) is an EBM and Eq. (1b) is an ice-sheet model (ISM). The '$\simeq$' symbol stands for a binary relation of rough proportionality and is intended to neglect the details of the equation's right-hand side (RHS), including its nonlinearities. The EBM represents the well-known ice-albedo feedback used by both Budyko (1969) and Sellers (1969), while the ISM relies on the precipitation-temperature feedback postulated by KCG and used also by Ghil and Le Treut (1981), who coined the term.

The latter feedback can be better understood by writing

$$\dot{V} \simeq p, \tag{2a}$$

$$p \simeq p_{\mathrm{ac}} - p_{\mathrm{ab}}, \tag{2b}$$

$$p_{\mathrm{ac}} \simeq T. \tag{2c}$$

Here p is net precipitation on the single ice sheet of the globally integrated model, given by the difference in Eq. (2b) between the accumulation p_{ac} and the ablation p_{ab} (KCG).

As first observed by George C. Simpson — the meteorologist of Robert F. Scott's *Terra Nova* expedition to the Antarctica in 1910–1912 and later the longest serving Director of the U.K. Meteorological Office — warmer winters have more snow and hence, at least in central Antarctica, the increase of p_{ac} with T exceeds the more obvious increase of p_{ab} with T. Hence $p \simeq T$ and we have derived therewith Eq. (1b), $V \simeq p \simeq T$. For more recent studies of the precipitation-temperature feedback, see Tziperman and Gildor (2002).

More generally, the presence of feedbacks of opposite sign in a system of two linear coupled ODEs

$$\dot{x} = y, \qquad \dot{y} = -x,$$

leads to an oscillation, with the solution given by two trigonometric functions in quadrature with each other, $x(t) = \sin(t)$, $y(t) = \cos(t) = \sin(t + \pi/2)$, and the trajectory describing a circle in the (x, y) phase plane, $x^2(t) + y^2(t) = 1$. In a nonlinear system, however — like the ~~full~~ KCG model or any other climate oscillator mentioned so far — the possibility of an oscillation, as indicated by the system (1), is actually realized in the explicit, full set of equations only for certain parameter values and not for others.

This can be understood by considering the so-called normal form of a *Hopf bifurcation*, which leads from a stable steady state, called a fixed point in dynamical systems theory, to a stable oscillatory solution, called a limit cycle. The easiest way to see this transition is by writing the normal form in polar coordinates, as in ~~Arnold (2012) and in Ghil and Childress (1987, Sec. 12.2)~~ Arnold (2012) and in Ghil and Childress (1987, Sect. 12.2), namely,

$$\dot{z} = (\mu + \imath\omega)z + c(z\bar{z})z. \tag{3}$$

Here $z = x + \imath y$ is complex, ~~with~~ where $\imath = \sqrt{-1}$ is the imaginary unit, while μ is a real bifurcation parameter, and c, ω are real and nonzero. Note that the KCG model per se is not in the normal form above and we will discuss its bifurcation parameter μ_* in the next subsection.
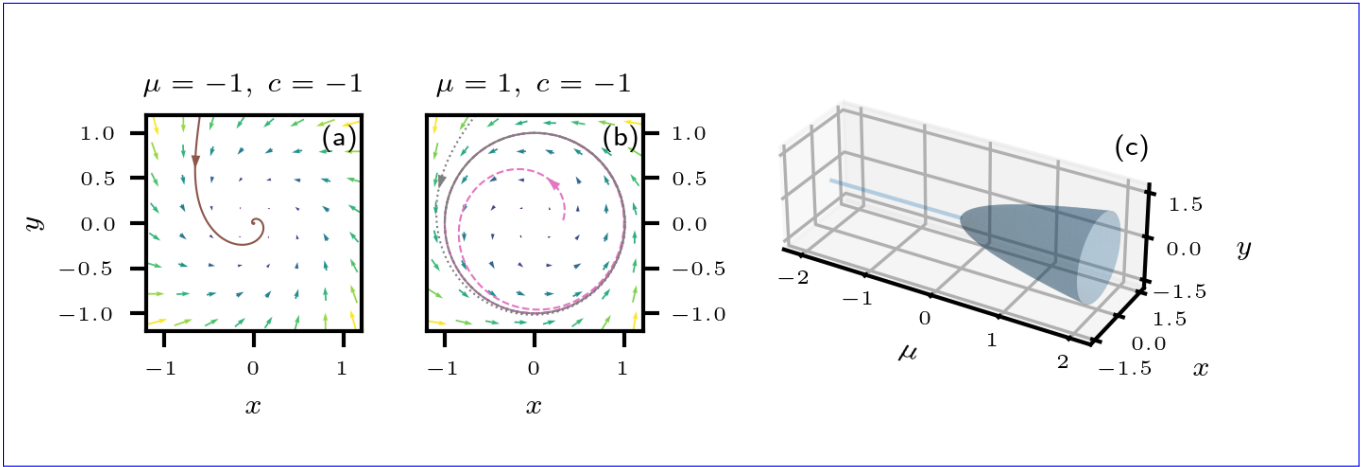
Figure 4. Supercritical Hopf bifurcation. (a) Vector field $\dot{z}(z)$ of Eq. (3) for the parameter values $\mu = -1$ and $c = -1$; $z = x + \imath y$. In this case, the origin constitutes the only stable fixed point and all trajectories will spiral into this point, as illustrated by the single brown trajectory. (b) Vector field $\dot{z}(z)$ and 3 trajectories for $\mu = 1$. In this case, the origin is an unstable fixed point, while the limit cycle with radius $\rho_*^{1/2} = 1$ constitutes the only stable solution. Trajectories that start inside this limit cycle, with $\rho(t_0) < \rho_*$, tend to it by spiraling out — as illustrated by the magenta trajectory — while trajectories that start outside the limit cycle, with $\rho(t_0) > \rho_*$, approach it by spiraling inward, as illustrated by the gray trajectory. (c) Dependence of the stable solution of Eq. (3) on the parameter μ, for $c = -1$. For $\mu \leq 0$, the single stable solution is the fixed point located at the origin, $\rho \equiv 0$. For $\mu > 0$, the stable solution is the limit cycle given by $\rho = \mu$.

A very natural transformation of variables,

$$\rho = z\bar{z} > 0, \quad z = \rho^{1/2} \exp(\imath\theta) \tag{4}$$

leads from the complex ODE (3) to the system of two real and decoupled ODEs,

$$\dot{\rho} = 2\rho(\mu + c\rho), \tag{5a}$$

$$\dot{\theta} = \omega. \tag{5b}$$

Equation (5b) simply provides an angular rotation around the origin $\rho = 0 = x = y$, since the complex exponential in Eq. (4) is periodic with period 2π. Equation (5a) is quadratic in ρ and thus it can have two real roots, $\rho = \rho_0 = 0$ and $\rho = \rho_* = -\mu/c$. But ρ has to be positive and so, in the case in which $c < 0$, the only possible solution for $\mu < 0$ is the origin and it is stable, since $\rho(\mu + c\rho)$ is negative for $\rho > 0$, in this case; hence, ρ has to be monotonically decreasing, i.e., all the solutions of Eq. (5) spiral into the origin. The Hopf bifurcation from this stable steady state to a periodic solution ~~with radius $\rho = \rho_*$~~, i.e., a limit cycle with radius $\rho^{1/2} = \rho_*^{1/2}$, occurs as μ crosses 0~~, and this solution is stable, since~~. Since now $\rho(\mu + c\rho) > 0$ for $0 < \rho < \rho_*$ and $\rho(\mu + c\rho) < 0$ for $\rho > \rho_*$, ~~i.e. solutions will~~ the limit cycle is stable and trajectories spiral out from inside ~~the limit~~ this cycle and into it from ~~the~~ outside; see ~~Ghil and Childress (1987, Fig. 12.7)~~ Fig. 4 for the so-called supercritical, or soft, Hopf bifurcation case with $c < 0$.

2.2 Intrinsic Climate Oscillations and the Mid-Pleistocene Transition (MPT)

In this subsection, we present an argument for the role of intrinsic oscillations in the mid-Pleistocene transition (MPT). The
150 ~~argument starts~~ first point to be made is that — while orbital forcing clearly plays a major role in the power spectrum of the
Quaternary's climatic variability — it cannot be, in and of itself, the cause of the MPT. Indeed, changes in the solar system's
orbital periodicities only occur on much longer time scales than the entire Quaternary's duration (Varadi et al., 2003; Laskar et al., 2004)
. Our argument continues with a further analysis of the Hopf bifurcation presented in the previous subsection. Such an analysis
was carried out for the KCG model by Ghil and Tavantzis (1983).

155 Physically speaking, the presence or absence of the regular, purely periodic oscillations obtained by KCG and illustrated
in Ghil and Childress (1987, Fig. 12.6) depends on whether $c \gtrless 0$ in Eq. (5a). The KCG model's bifurcation parameter is
$\mu_* = c_T/c_L$, where c_T is the heat capacity in its EBM, while c_L is the "mass capacity" in its ISM (Ghil and Tavantzis, 1983).
Large μ_* corresponds physically to a very small, possibly pre-Pleistocene ice cap (Ghil, 1984; Saltzman and Sutera, 1987). At
these values of μ_*, the KCG model's isoclines and fixed points — the latter being given by the intersection of the former — are
160 very different from those that are obtained for Quaternary-size ice sheets, for which c_L is comparable in value to c_T; see Ghil
and Tavantzis (1983, Figs. 3–5). As μ_* decreases to $O(1)$, i.e., as we proceed from very small to more substantial ice sheets,
the fixed point transfers its stability to a branch of periodic solutions, by a subcritical Hopf bifurcation (Källén et al., 1979;
Ghil and Tavantzis, 1983); see also Ghil and Childress (1987, Figs. 12.8 and 12.9).

To clarify the simple physical concepts that underlie sub- and supercritical Hop bifurcations, let us consider a purely me-
165 chanical oscillator with mass m, a spring kx and a dashpot $\alpha\dot{x}$ (Landau and Lifshitz, 1960; Jordan and Smith, 1987),

$$m\ddot{x} = -\alpha(x)\dot{x} - k(x)x. \tag{6}$$

If $k =$ const. and $\alpha =$ const., we have the simplest, linear setup, but we will be interested here in the nonlinear cases. Normalizing
by the mass m and not changing notation otherwise, we get by rearranging terms and adding a periodic forcing

$$\ddot{x} + \alpha(x)\dot{x} + k(x)x = F\cos(\omega t). \tag{7}$$

170 Two classical nonlinear cases are those of the ~~Duffing (1918)~~ Duffing (1918) equation, in which $k(x) = x^2$ and $\alpha =$ const.,
and of the ~~Van der Pol (1926)~~ Van der Pol (1926) equation, in which $k =$ const. and $\alpha(x) = \nu(x^2 - 1)$. The fully nonlinear
case in which both the spring and the damping are nonlinear, with $k(x) = x^2$ and $\alpha(x) = \nu(x^2 - 1)$, is known as the Van der
Pol–Duffing oscillator (e.g., Jackson, 1991; Pierini et al., 2018). Note that all three types of nonlinear oscillators can exhibit
chaotic behavior even in the presence of simply periodic forcing (e.g., Guckenheimer and Holmes, 1983; Pierini et al., 2018,
175 and references therein). The idea of using such simple, classical oscillators in modeling Quaternary glaciation cycles goes back
to Saltzman et al. (1981).

~~Jordan and Smith (1987, Sec. 5.6)~~ Jordan and Smith (1987, Sect. 5.6) discuss specifically the case of a soft and a hard spring
for a generalized Duffing equation, with $k(x) = k_0 + \epsilon h(x)$, where ~~$0 < \epsilon \ll 1, h(-x) = h(x), h' \geq 0,$~~ $0 < |\epsilon| \ll 1, h(-x) = h(x),$
and $h'' > 0$. A spring is soft if it is sublinear, $\epsilon < 0$, and hard if it is superlinear, $\epsilon > 0$; see their Eq. (5.37) and Figs. 5.4(a,b),
180 with $h(x) = x^2$.

The supercritical Hopf bifurcation ~~corresponds to~~ in the absence of forcing is analogous to the nonlinear response of a soft, sublinear spring to periodic forcing in which the oscillations in the position x of the mass m increase gradually in amplitude as the spring constant k_0 increases past a critical value k_*, while the subcritical case ~~corresponds to~~ is analogous to the response of a hard, superlinear spring, ~~where~~ for which the oscillations in x jump suddenly from zero amplitude to a finite amplitude as the spring constant k_0 crosses the value k_*. Please compare the behavior of supercritical and subcritical Hopf bifurcations in Ghil and Childress (1987, Sect. 12.2 and Figs. 12.7–12.9)) and see Jordan and Smith (1987, Fig. 5.7) for the change in the nonlinear response of a Duffing oscillator as its spring changes from soft, with $\epsilon < 0$, to hard, with $\epsilon > 0$.

There is a clear-cut analogy with the mid-Pleistocene transition, occurring at roughly 0.8 ~~Myr~~Ma b2k, at which small-amplitude climate variability with a dominant periodicity near 40 kyr becomes larger, dominated by a periodicity that is close to 100 kyr, as well as being more irregular ~~(e.g., Huybers, 2009; Rousseau et al., 2022)~~(e.g., Huybers, 2009; Quinn et al., 2017; Rousseau et a. A fair number of distinct dynamical theories for this transition have been formulated ~~(e.g., Ghil, 1994; Crucifix, 2012; Ashwin and Ditlevs~~(e.g., Maasch and Saltzman, 1990; Ghil, 1994; Crucifix, 2012; Ashwin and Ditlevsen, 2015; Daruka and Ditlevsen, 2016; Omta et al., 201. A rather obvious one is that a Hopf bifurcation occurs at that point, which leads to a more vigorous response to the multiperiodic orbital forcing; thus, the latter does not need to change in the least in order to explain the observed phenomena. In Saltzman and Sutera (1987), there is only a comment on the likely role of a Hopf bifurcation in the transition, but their Fig. 3 suggests that, in their model, such a bifurcation would have to be of the supercritical type, and lead to a fairly gradual transition.

To the contrary, the subcritical Hopf bifurcation of the KCG and Ghil and Le Treut (1981) oscillators would have to lead to a more abrupt transition, as suggested by Ghil (1984). Later Crucifix (2012) showed that the models by Saltzman and Maasch (1990, 1991) exhibit MPT-like behavior via supercritical or subcritical Hopf bifurcations, depending on the parameter values. The existing δ^{18}O and δ^{13}C records might or might not have sufficient resolution back in time up to 1.2 Ma to settle this question about the abruptness of the transition. In case some of them do, an objective test of suddenness ~~,~~ as proposed by Bagniewski et al. (2021) for the high-resolution NGRIP record (North Greenland Ice Core Project members, 2004) ~~,~~ will have to be applied to such records.

3   TIME-DEPENDENT FORCING, NDSS AND RDSS

3.1   Orbital Forcing of a Climate Oscillator

We start this section by describing some fairly simple ways in which the orbital forcing might have ~~interacted with~~ modified intrinsic climate variability, thus helping to solve the mismatch between Figs. 3(a) and 3(b) in ~~Section~~Sect. 1. To explore this possibility, Le Treut and Ghil (1983) used somewhat simplified insolation forcing, based on the calculations of Berger (1978), and applied it to a slightly modified version of the Ghil and Le Treut (1981) oscillator. These authors found that, as expected for a nonlinear oscillator, its internal frequency f_0 ~~interacts with~~ is affected strongly by the forcing ones, $\{f_1, \ldots, f_5\}$, ~~to produce~~ resulting in both nonlinear resonance and combination tones (Landau and Lifshitz, 1960).

Depending on parameter values, the periodicity $P_0 = 1/f_0$ of the Ghil and Le Treut (1981) oscillator is $P_0 \simeq 6\text{–}7$ kyr. The lines in the simplified insolation spectrum used by Le Treut and Ghil (1983) had the periodicities

$$P_1 = 19 \text{ kyr}, \ P_2 = 23 \text{ kyr}, \ P_3 = 41 \text{ kyr}, \ P_4 = 100 \text{ kyr}, \text{ and } P_5 = 400 \text{ kyr}; \qquad (8)$$

215 these periodicities correspond to the two precessional ones, the obliquity one, and two eccentricity ones. The actual ~~celestial mechanics~~ celestial-mechanics calculations that Berger (1978) based his insolation calculations on have been substantially updated since (e.g., Varadi et al., 2003; Fienga et al., 2015). But these advances have not modified much the spectrum of the planetary-orbit solutions over the 2.6 Myr of the Quaternary, a rather short interval in celestial-mechanics terms.

The results of the Le Treut and Ghil (1983) model on the evolution of the primary climate variables T and V were converted
220 to $\delta^{18}O$ values in simulated isotopic records of marine-sediment and ice cores by Le Treut et al. (1988); the spectra of the latter are plotted in Fig. 5. The values on the abscissa of Fig. 5(a) are values of the logarithm of frequency, while those in Fig. 5(b) are values of the frequency itself; the values on the ordinate of both panels are powers of 10. One refers to such figures as being in (a) log-log coordinates vs. (b) log-linear coordinates for short.

Aside from the spectral features noted in the figure caption and discussed in greater detail by Ghil (1994), it is important
225 to realize (i) that the large continuous background in Fig. 5(a) is purely of deterministically chaotic origin, since there is no stochastic element whatsoever in the Le Treut and Ghil (1983) model or in its forcing; and (ii) that the dominant peak at 109 kyr is not directly forced by the $f_4 = 1/100 \ (\text{kyr})^{-1}$ eccentricity line but rather it is due to the difference tone between the two precessional frequencies, f_1 and f_2. Finally, it is the nonlinear, broad resonance of the model's f_0 frequency with the quasi-periodic forcing that produces the bump in the spectrum of Fig. 5(a) to the right of the orbital frequencies.

230 In returning to the "fundamental question #2" in **Box 1**, one must recall that, on the paleoclimatic time scales of interest — apart from deterministic chaos à la ~~Lorenz (1963)~~Lorenz (1963), as obtained by H. Le Treut and colleagues (Le Treut and Ghil, 1983; Le Treut et al., 1988) and shown here in Fig. 5(a) — stochastic contributions à la ~~Hasselmann (1976)~~ Hasselmann (1976) to the continuous part of the ~~paleoclimatic~~ spectrum must also play an important role. In fact, ~~the theory of random dynamical systems touched upon~~ RDS theory, as outlined in the next subsection, provides an excellent framework for a "grand unifi-
235 cation" of these two complementary points of view (Ghil, 2014, 2019). In the paleoclimatic context, ~~Ditlevsen et al. (2020)~~ Ditlevsen et al. (2020) have suggested that, aside from red-noise processes, dating uncertainties in the proxy records from which the spectra are derived may contribute, in all likelihood, to this background; see also ~~Boers et al. (2017a, b).~~

Boers et al. (2017a, b). In this context, Verbitsky and Crucifix (2020) also provide a simple theory that addresses scaling properties in the glacial cycles and their spectra, based on the so-called Buckingham π-theorem (e.g., Barenblatt, 1996).

240 ## 3.2 Basic Facts of NDS and RDS Life

The highly preliminary results ~~on interaction between external forcing and internal variability summarized in Sec~~summarized in Sect. 3.1 encourage us to pursue in a more systematic way the ~~interaction between orbital forcing and~~ effects of the orbital forcing on intrinsic climatic variability, effects that may have contributed to generate the rich paleoclimate spectrum on Quaternary and longer time scales (e.g., Westerhold et al., 2020). In fact, several research groups in the climate sciences have carried
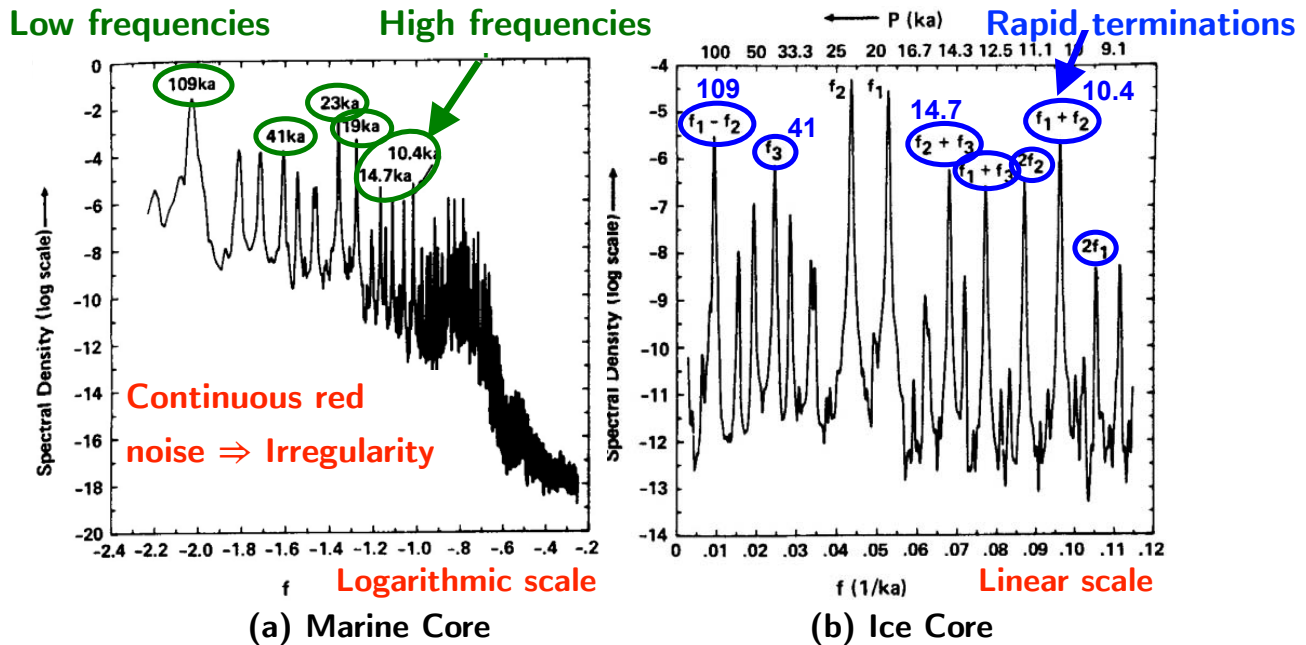
Figure 5. Power spectra of simulated (a) deep-sea and (b) ice core records for the forced climate oscillator of Le Treut and Ghil (1983) with idealized orbital forcing. Panel (a) is in log-log coordinates and clearly shows a dominant peak at 109 kyr and a very large amount of variance in the continuous spectrum, which has a roughly -2 power law slope. The orbital peaks at $P_1 = 19$ kyr, $P_2 = 23$ kyr and $P_3 = 41$ kyr are also present along with peaks at 14.7 kyr and 10.4 kyr, which correspond to the sum tones $f_2 + f_3$ and $f_1 + f_2$, respectively. Panel (b) is in log-linear coordinates and shows additional harmonics and sum tones, as well as the difference tone $f_1 - f_2$, which corresponds to the dominant peak at 109 kyr. ~~After Le Treut et al. (1988) with permission~~ Adapted by permission from John Wiley & Sons Inc.: American Geophysical Union. Journal of Geophysical Research: Atmospheres. Orbital Forcing, Climatic Interactions, and Glaciation Cycle by Le Treut and Ghil; Copyright 1983 by the American Geophysical Union. (1983)

245   out during the past two decades an important extension of the dynamical-systems and model hierarchy framework presented by Ghil and Childress (1987) and by Ghil (2001), from deterministically autonomous to nonautonomous and random dynamical systems (NDSs and RDSs: e.g., Ghil et al., 2008; Chekroun et al., 2011; Bódai and Tél, 2012).

     On the road to including deterministically time-dependent, as well as random effects, one needs to realize first that the climate system — as well as any of its subsystems, and on any time scale — is not closed: it exchanges energy, mass and momentum

250   with its surroundings, whether other subsystems or the interplanetary space and the solid earth. The typical applications of dynamical systems theory to climate variability until not so long ago have only taken into account exchanges that are constant in time, thus keeping the model — whether governed by ordinary, partial or other differential equations — autonomous; i.e., the models had coefficients and forcings that were constant in time.

Alternatively, the external forcing or the parameters were assumed to change either much more slowly than a model's internal variability, so that the changes could be assumed to be quasi-adiabatic, or much faster, so that they could be approximated by stochastic processes. Some of these issues are covered in much greater detail by ~~Ghil and Lucarini (2020, Sec. III.G)~~ Ghil and Lucarini (2020, Sect. III.G). The key concepts and tools of NDSs and RDSs go beyond such approaches that rely in an essential way on a scale separation between the characteristic times of the forcing and the internal variability of a given system; such a separation is rarely, if ever, actually present in the climate sciences.

The presentation of the key NDS and RDS concepts and tools in this subsection is aimed at as large a readership as possible and it follows Ghil (2014). Slightly more in-depth, but still fairly expository presentations can be found in Crauel and Kloeden (2015) and in Caraballo and Han (2017). Readers who are less interested in this mathematical framework — which allows a truly thorough understanding of the way that orbital forcing ~~interacts with~~ acts on intrinsic climate variability on Quaternary time scales — may skip at a first reading the remainder of this section and continue with ~~Section~~Sect. 4.

Autonomous and nonautonomous systems. Succinctly, one can write an autonomous system as

$$\dot{\mathbf{X}} = \mathbf{F}(\mathbf{X}; \mu), \tag{9}$$

where $\mathbf{X}$ stands for any state vector or climate field. While $\mathbf{F}$ is a smooth function of $\mathbf{X}$ and of the parameter μ, it does not depend explicitly on time. This autonomous character of Eq. (9) greatly facilitates the analysis of its solutions' properties.

For instance, two distinct trajectories, $\mathbf{X}_1(t)$ and $\mathbf{X}_2(t)$, of a well-behaved, smooth autonomous system cannot intersect — i.e., they cannot pass through the same point in phase space — because of the uniqueness of solutions. This property helps one draw the phase portrait of an autonomous system, as does the fact that we only need to consider the behavior of solutions $\mathbf{X}(t)$ as time t tends to $+\infty$. The sets of points so obtained are — possibly multiple — equilibria, periodic and quasi-periodic solutions, and chaotic sets. In the language of dynamical systems theory, these are called, respectively: *fixed points, limit cycles, tori,* and *strange attractors.*

We know only too well, however, that the seasonal cycle plays a key role in climate variability on interannual time scales, while orbital forcing is crucial on the Quaternary time scales of many millennia. And, more recently, it has become obvious that anthropogenic forcing is of utmost importance on the interdecadal time scales in-between.

How can one take into account these types of time-dependent forcings, and analyze the nonautonomous systems that they lead us to formulate? One writes succinctly such a system as

$$\dot{\mathbf{X}} = \mathbf{F}(\mathbf{X}, t; \mu). \tag{10}$$

In Eq. (10), the dependence of $\mathbf{F}$ on t may be periodic, $\mathbf{F}(\mathbf{X}, t + P) = \mathbf{F}(\mathbf{X}, t)$, as in various El Niño–Southern Oscillation (ENSO) models, where the period $P = 12$ months, or ~~monotone, $\mathbf{F}(\mathbf{X}, t + \tau) \geq \mathbf{F}(\mathbf{X}, t)$~~monotonic, $|\mathbf{F}|(\mathbf{X}, t + \tau) \geq |\mathbf{F}|(\mathbf{X}, t)$, as in studying scenarios of anthropogenic climate forcing. An even more general situation includes time dependence in one or more parameters $\{\mu_1, \ldots, \mu_p\}$.

To illustrate the fundamental distinction between an autonomous system like Eq. (9) and a nonautonomous one like Eq. (10), consider the simple scalar version of these two equations:

$$\dot{X} = -\beta X, \qquad \text{and} \tag{11a}$$

$$\dot{X} = -\beta X + \gamma t, \tag{11b}$$

respectively. We assume that both systems are dissipative, i.e. $\beta > 0$, and that the forcing is ~~monotone~~ monotonically increasing, $\gamma \geq 0$, as would be the case for anthropogenic forcing in the industrial era. Lorenz (1963) pointed out the key role of dissipativity in giving rise to strange, but attracting solution behavior, while Ghil and Childress (1987) emphasized its importance and pervasive character in climate dynamics. Clearly the only attractor for the solutions of Eq. (11a), given any initial point $X(0) = X_0$, is the stable fixed point $X_* = 0$, attained as $t \to +\infty$.

In the case of Eq. (11b), though, this forward-in-time approach yields blow-up as $t \to +\infty$, for any initial point. To make sense of what happens in the case of time-dependent forcing, one introduces instead the *pullback approach*, in which solutions are allowed to still depend on the time t at which we observe them, but also on a time s from which the solution is started, with $X(s) = X_0$ and $s \ll t$. With this little change of approach, one can easily verify that

$$|X(s,t;X_0) - \mathcal{A}_t| \to 0 \quad \text{as} \quad s \to -\infty, \tag{12}$$

for all t and X_0, where $\mathcal{A}_t = (\gamma/\beta)(t - 1/\beta)$. We obtain therewith, in this pullback sense, the intuitively obvious result that the solutions, if we start them far enough in the past, all approach the family of attracting sets $\mathcal{A}_t$; this family follows the forcing γt and it thus has a linear growth in time t. Hence, the fixed point X_* of Eq. (11b) is, in fact, a moving target and it is given by $X_* = \gamma t/\beta$. Due to the system's inertia, the set $\mathcal{A}_t$ that is approached by the trajectories lags this time-dependent fixed point by a constant offset of γ/β^2.

Pullback attractor (PBA). Formally, the indexed family $\mathscr{A}$ of all pullback attracting sets $\mathcal{A}_{t,}$

$$\mathscr{A} = \{\mathcal{A}_t\}_{t \in \mathbb{R}} \tag{13}$$

is termed the *pullback attractor* (PBA) of the NDS if the following two conditions are fulfilled:

(i) each snapshot $\mathcal{A}_t$ is compact and the family of snapshots ~~$\{\mathcal{A}(t)\}_{t \in R}$~~ $\{\mathcal{A}(t)\}_{t \in \mathbb{R}}$ is invariant with respect to the dynamics

$$X(t,s;X_0) \in \mathcal{A}_t \quad \forall s \leq t \text{ and } X_0 \in A_s; \text{ and} \tag{14}$$

(ii) the pullback attraction occurs for all times:

$$\lim_{s \to -\infty} |X(t,s;X_0) - \mathcal{A}_t| = 0 \quad \forall t. \tag{15}$$

To further improve the reader's intuition for PBAs, we provide a second illustrative example here. A system defined in polar coordinates by

$$\dot{\rho} = \alpha(\mu - \rho), \quad \dot{\phi} = \omega, \quad \text{with } \rho, \mu \in \mathbb{R}^+ \text{ and } \phi \in \mathbb{R}/2\pi, \tag{16}$$

14

can easily be seen to exhibit a limit cycle in the (x,y)-plane with $(x = \rho\cos\phi, y = \rho\sin\phi)$. An initial deviation of ρ from μ will decay exponentially and the system converges to an oscillation of radius μ with the angular velocity ω. Here, we transform this autonomous dynamical system into a nonautonomous one by modulating the target radius μ with a sinusoidal forcing

$$\mu \to \mu(t) = \mu_0 + \beta\sin(\nu t), \tag{17}$$

where the modulation is moderate, so as to guarantee that ~~$\mu + \beta\sin(\nu t) > 0$~~ $\mu_0 + \beta\sin(\nu t) > 0$ for all t.

Since the dynamics of the phase ϕ and of the radius ρ are decoupled, the corresponding equations can be solved and analyzed separately. While the temporal development of the phase is trivial, the pullback invariant attracting set of the radius for the initial condition $\rho(s) = \rho_0$ is given by

$$\mathcal{A}^{(\rho)}(t;\rho_0) = \lim_{s\to-\infty}\rho(t,s;\rho_0) = \alpha\beta\sin(\nu t + \vartheta) + \mu_0, \quad \text{with} \tag{18a}$$

$$\vartheta = \arctan(-\nu/\alpha), \tag{18b}$$

as shown in Appendix B. Note that, in the limit $s\to-\infty$, the dependence on the initial value ρ_0 vanishes and the attracting set $\mathcal{A}_t^{(\rho)}$ performs an oscillation of the same frequency as the forcing. It lags the phase of the time-dependent fixed point by the constant ϑ, while its amplitude is amplified by the factor α. Since ρ is restricted to positive values, this solution requires ~~$\alpha\beta < \mu$~~ $\alpha\beta \leq \mu_0$.

The PBA with respect to the coordinate ρ is comprised of the family of all the sets $\mathcal{A}_t^{(\rho)}$ as defined in (18) and thus reads

$$\mathscr{A}^{(\rho)} = \{\alpha\beta\sin(\nu t + \vartheta) + \mu_0\}_{t\in\mathbb{R}}. \tag{19}$$

Since the pullback limit for the phase ϕ does not exist, no constraints on it other than $\phi \in [0, 2\pi)$ are imposed by the dynamics. Hence, for the system (16) comprised of radius and phase, we find that

$$\lim_{t_0\to-\infty} d_{\mathrm{H}}\left((\rho(t;t_0,\rho_0),\phi(t;t_0,\phi_0)), \underbrace{\{(\alpha\beta\sin(\nu t + \vartheta) + \mu, \varphi) : \varphi \in [0,2\pi)\}}_{\mathcal{A}_t}\right) = 0,$$

~~where d_{H} denotes the Hausdorff semi-distance~~ the distance of any trajectory at time t — i.e. $(\rho(t;t_0,\rho_0),\phi(t;t_0,\phi_0))$ — to the set $\mathcal{A}_t = \{(\alpha\beta\sin(\nu t + \vartheta) + \mu_0, \varphi) : \varphi \in [0,2\pi)\}$ tends to zero, as we pullback the initial time t_0 to $-\infty$. The pullback attracting sets $\mathcal{A}_t$ at time t are circles in the (x,y)-plane with ~~oscillating radius~~ a radius that oscillates in time, and the system's PBA is given by the family of these circles

$$\mathscr{A} = \{(\alpha\beta\sin(\nu t + \vartheta) + \mu_0, \varphi) : \varphi \in [0,2\pi)\}_{t\in\mathbb{R}}. \tag{20}$$

Figure 6 shows trajectories of the system starting from different points in the past. In panel (a), the trajectories are depicted in the three-dimensional (3-D) space spanned by the two cartesian coordinates (x,y) and the time t, where the usual transformation from polar to cartesian coordinates was applied. The shaded surface in this panel represents the PBA of the system. ~~Panel~~ Corresponding trajectories of $\rho(t)$ and their convergence to the PBA $\mathcal{A}_t^{(\rho)}$ are shown in panel (b). Panel (f) shows a heat map

(Wilkinson and Friendly, 2009) that approximates a portion of the PBA's invariant measure projected onto the (x,y)-plane. For a clean definition of such a measure in NDSs and RDSs, please see Caraballo and Han (2017); Chekroun et al. (2011); Crauel and Kloeden (2015) or Ghil et al. (2008). Essentially, the heat map here counts the number of times that 100 trajectories integrated from $t = -200$ to $t = 200$, with randomized initial conditions like the ones shown in panel (a), cross small pixels in the (x,y)-plane.

Panels (c–e) demonstrate a particularity of this system, which is characteristic of dynamics confined to a torus. Namely, the structure of the system's trajectories depends on the frequency ratio ω/ν and three different cases must be distinguished. If the radius is modulated with the same frequency as the oscillation itself, i.e. $\omega = \nu$ as in panel (c), the forcing and the system have a fixed phase relation. That is, for a given phase of the system, its radius is always attracted by the same fixed point. Hence, the system practically repeats its orbit after a short time. More precisely, the radius of the oscillation does differ from one "roundtrip" around the torus to the next, but this difference tends to zero as $\rho(t)$ approaches the PBA $\mathcal{A}_t^{(\rho)}$.

If ω and ν are rationally related, i.e., $m\omega = n\nu$ with $n, m \in \mathbb{N}$, as in panel (d), then — after n periods of the radial modulation and m periods of the system's oscillation — the phase relation between the system and its forcing will repeat itself and hence we observe the same quasi-repetition of the orbit after the time $n\,2\pi/\nu = m2\pi/\omega$. That is, such a trajectory will appear as an n-fold quasi-closed loop.

Finally, if $\omega/\nu \notin \mathbb{Z}$, as in panel (e), then a given phase of the system will never coincide with the same phase of the radius modulation more than once. Hence, the trajectory does not repeat itself but instead covers densely the annular disc $\mathcal{D} = \{(\rho, \phi) : \rho \in [\mu_0 - \alpha\beta, \mu_0 + \alpha\beta] \text{ and } \phi \in [0, 2\pi)\}$.

Random attractor. Let us return now to the more general, nonlinear case of Eq. (10) and add not only deterministic time dependence $\mathbf{F}(\mathbf{X}, t)$, but also random forcing,

$$\mathrm{d}\mathbf{X} = \mathbf{F}(\mathbf{X}, t)\mathrm{d}t + \mathbf{G}(\mathbf{X})\mathrm{d}\eta, \tag{21}$$

where $\eta = \eta(t, \omega)$ represents a Wiener process — with $\mathrm{d}\eta$ commonly referred to as "white noise" — and ω now labels the particular realization of this random process. When $\mathbf{G} = \text{const.}$ the noise is additive, while for $\partial\mathbf{G}/\partial\mathbf{X} \neq 0$ we speak of multiplicative noise. The distinction between $\mathrm{d}t$ and $\mathrm{d}\eta$ in the stochastic differential equation (21) is necessary since, roughly speaking and following the Einstein (1905) paper on Brownian motion, it is the variance of a Wiener process that is proportional to time and thus $\mathrm{d}\eta \propto (\mathrm{d}t)^{1/2}$. In Eq. (21), we dropped the dependence on a parameter μ for the sake of simplicity.

The noise processes may include "weather" and volcanic eruptions when $\mathbf{X}(t)$ is "climate," thus generalizing the linear model of Hasselmann (1976), or cloud processes when dealing with the weather itself: one person's signal is another person's noise, as the saying goes. In the case of random forcing of Eq. (21), the concepts introduced by the simple deterministic examples of Eq. (11b) and of Eqs. (16, 17) above can be illustrated by the *random attractor* $\mathscr{A}(\omega)$ in Fig. 7.
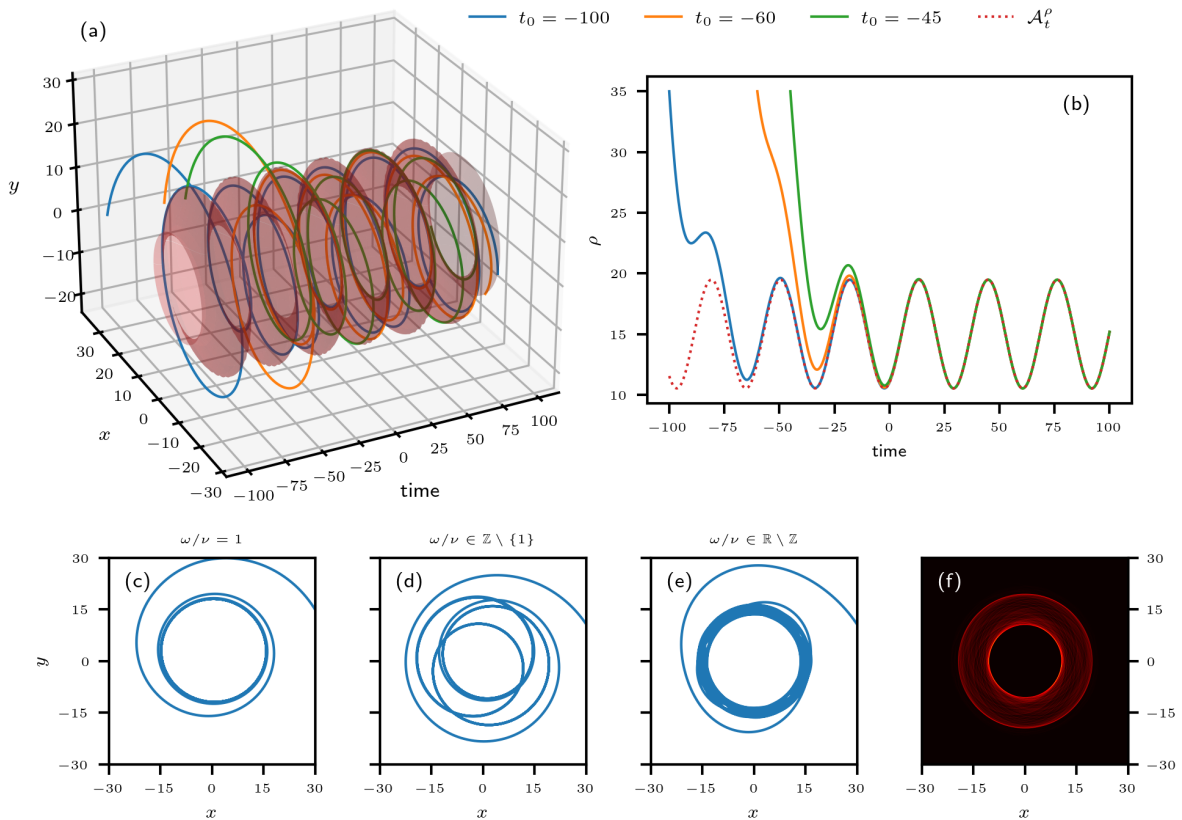
Figure 6. Trajectories and PBA of the system defined by Eqs. (16) and (17); in all the panels the parameter values are $\mu_0 = 15$, $\alpha = 10$, $\nu = 0.2$ and $\omega = 0.3$, unless stated otherwise. (a) Trajectories $(\rho(t), \phi(t))$ of the system starting from different times in the past in the 3-D space spanned by the two cartesian coordinates (x, y) and time t; the system's PBA lies on the red-shaded surface. (b) Temporal evolution of the radius (solid colors) of the three trajectories shown in (a) together with its PBA (dotted red). (c)–(e) Trajectories integrated from $t_0 = -100$ to $t_f = 200$ for $\nu = 0.3, 0.2, 0.5^{1/2}$ in panels (c), (d) and (e), respectively. The values are chosen such that the ratio between ν and ω is $\omega/\nu = 1$, $\omega/\nu \in \mathbb{Z} \setminus \{1\}$ and $\omega/\nu \in \mathbb{R} \setminus \mathbb{Z}$ in panels (c) to (e), respectively. Correspondingly, in (c) the trajectory quickly converges to a circle, whose center is slightly shifted from the originin. In panel (d) a quasi-closed three-fold loop can be observed, since $\omega/\nu = 3/2$. In panel (e) the trajectories will densely fill the annular disc defined by Eq. (32). (f) Heat map of the numerous trajectories projected onto the (x, y)-plane. The trajectories start at random points in state space and are integrated from $t_i = -200$ to $t_f = 200$. A video of the heat map filling up, as more and more trajectories with different initial conditions are added, is provided in the Supplementary Material to this article. The heat map shown here is a snapshot of the video taken at time $t = 0.20$; see details in the Video video supplement. (c) Temporal evolution of the phase. (d) Temporal evolution of the radius (solid colors) together with its PBA (dotted red).

A key feature of the pullback point of view on noise-perturbed dynamical systems that characterizes RDS theory is the use of a single noise realization, as opposed to the traditional, forward viewpoint of the Fokker-Planck equation and associated concepts, in which multiple noise realizations play a role. For a precise definition of a random attractor — as well as the commonalities and differences between the deterministic and random cases of time-dependent forcing — please see Caraballo and Han (201
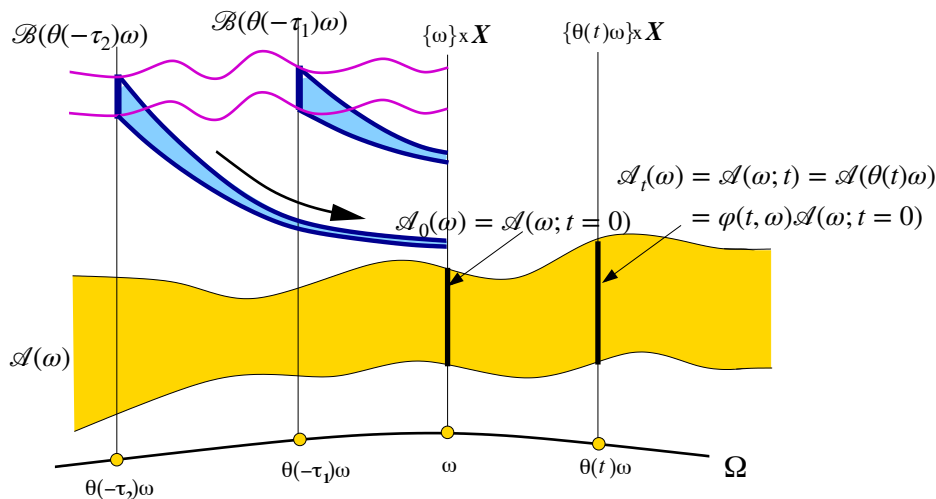
380 ~

Figure 7. Schematic diagram of a random attractor $\mathscr{A}(\omega)$ and of the pullback attraction to it; here ω labels the particular realization of the random process $\theta(t)\omega$ that drives the system. We illustrate the evolution in time t of the random process $\theta(t)\omega$ (light solid black line at the bottom); the random attractor $\mathscr{A}(\omega)$ itself (yellow band in the middle), with the *snapshots* $\mathcal{A}_0(\omega) = \mathcal{A}(\omega; t = 0)$) and $\mathcal{A}(\omega; t)$ (the two vertical sections, heavy solid); and the flow of an arbitrary compact set $\mathcal{B}$ from "pullback times" $t = -\tau_2$ and $t = -\tau_1$ onto the attractor (heavy blue arrows). See Ghil et al. (2008, Appendix A) for the requisite properties of the random process $\theta(t)\omega$ that drives the RDS (21).

Chekroun et al. (2011) studied a specific case of such a random attractor for the paradigmatic, climate-related Lorenz (1963) convection model. The authors introduced multiplicative noise into each of the ODEs of the original, deterministically chaotic system, as shown below:

$$\mathrm{d}X = P_r(Y - X)\mathrm{d}t + \sigma X \mathrm{d}\eta, \tag{22a}$$

385
$$\mathrm{d}Y = (rX - Y - XZ)\mathrm{d}t + \sigma Y \mathrm{d}\eta, \tag{22b}$$

$$\mathrm{d}Z = (-bZ + XY)\mathrm{d}t + \sigma Z \mathrm{d}\eta; \tag{22c}$$

here $r = 28$, $P_r = 10$, $b = 8/3$ are the standard parameter values for chaotic behavior in the absence of noise, and σ is a constant variance of the Wiener process that is not necessarily small; both the noise realization $\eta(t)$ and σ are the same in all three equations. The well-known strange attractor of the deterministic case is replaced by the Lorenz model's random attractor, dubbed LORA by the authors. Four *snapshots* $\mathcal{A}_t(\omega)$ of LORA are plotted in Fig. 8 and a video of its evolution in time $\mathscr{A}(\omega) = \{\mathcal{A}_t(\omega)\}_{t \in \mathbb{R}}$ is available as Supplementary Material in ~~Chekroun et al. (2011)~~ Chekroun et al. (2011) at https://doi.org/10.1016/j.physd.~~2011.06.005~~2011.06.005.

Charó et al. (2021) have further analyzed the striking effects of the noise on the nonlinear dynamics that are visible in Fig. 8 here and in the video of ~~Chekroun et al. (2011)~~Chekroun et al. (2011), and gathered further insights into the abrupt changes of the snapshots' topology at critical points in time. These remarkable changes suggest the possibility of random processes giving rise to qualitative jumps~~in paleoclimatic variability~~, such as the MPT, in paleoclimatic variability.

3.3 Application to Dansgaard-Oeschger (D-O) events

Before discussing conceptual glacial cycle models, we take a little detour and introduce a simpler — yet interesting and, at the same time, highly instructive — application of NDS theory to another important climate phenomenon. During past glacial periods, Greenland experienced a series of sudden decadal-scale warming events that left a clear trace in ice core records (Dansgaard et al., 1993). These so-called D-O events were followed by intervals of steady moderate cooling, before a short phase of enhanced cooling brought the temperatures back to their pre-event levels (e.g., Rasmussen et al., 2014). This pattern is very clearly apparent in NGRIP δ^{18}O records (North Greenland Ice Core Project members, 2004) and it can be ~~mimicked qualitatively~~ qualitatively simulated by the fast component of a FitzHugh-Nagumo (FHN) model (FitzHugh, 1961; Nagumo et al., 1962), as pointed out by ~~Mitsui and Crucifix (2017)~~Mitsui and Crucifix (2017), among others; see also ~~Kwasniok (2013); Rial and Yang (2007)~~Kwasniok (2013); Rial and Yang (2007); Roberts and Saha (2017); Vettoretti et al. (under review).

We discuss the example of the FHN model at some length in order to illustrate how external forcing can act on a system's internal variability and thereby give rise to more complex dynamics. This model's concise mathematical formulation and its widespread application in paleoclimate modeling and other fields make it ideally suited for this goal. We start with a description of the autonomous model, with no time-dependent forcing. Subsequently, we introduce a simple sinusoidal forcing and numerically compute the corresponding PBA. We then extend these consideration into the realm of random dynamical systems by adding stochastic forcing and discuss the resulting random attractor. Finally, we replace the synthetic forcings by one that corresponds to a paleoclimate proxy record of past CO_2 concentrations retrieved from Antarctic ice cores (Bereiter et al., 2015) and show that this setup brings the model's trajectories into good qualitative agreement with the D-O patterns observed in δ^{18}O records from Greenland ice cores. In doing so, we pay less attention to the physical interpretation of the model's variables, while focusing on the detailed explanation of model behavior and on the role of the forcing in the resulting dynamics.

The FitzHugh-Nagumo (FHN) model of ~~fast-slow~~ fast–slow oscillations. The FHN model consists of two coupled ODEs that govern behavior alternating between slow evolutions and fast transitions. Typically, the time scales of the two variables are
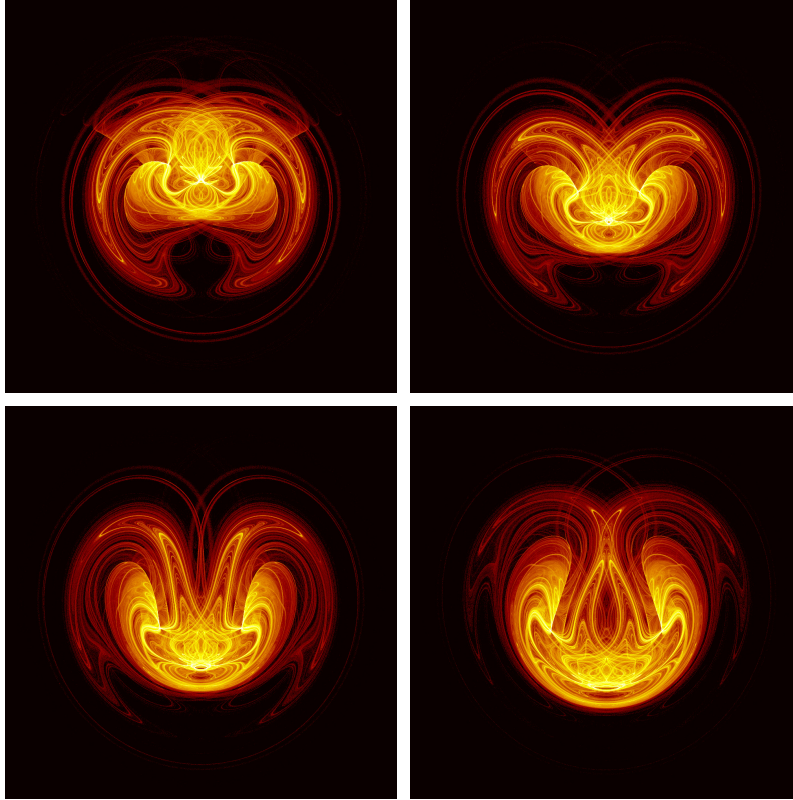
Figure 8. Heat maps of the time-dependent invariant measure $\nu_t(\omega)$ supported on four snapshots $\mathscr{A}_t(\omega)$ of LORA. The values of the parameters r, s and b are the classical ones, while the variance of the noise $\sigma = 0.5$. The color bar is on a log-scale and it quantifies the probability of landing in a particular region of phase space; shown is a projection of the 3-D phase space (X, Y, Z) onto the (X, Z)-plane. Note the complex, interlaced filament structures between highly populated regions (in yellow) and moderately populated ones (in red). ~~Reproduced~~ Reprinted from ~~Ghil et al. (2008)~~ Physica D: Nonlinear Phenomena, 240, Ghil et al., Stochastic climate dynamics: Random attractors and time-dependent invariant measures, 1685–1700, ©2011 Elsevier B.V. All rights reserved. (2011), with permission from Elsevier.

420   separated by introducing the parameters τ_x and τ_y, with $x(t)$ being the slow component and $y(t)$ the fast one:

$$\dot{x} = \frac{1}{\tau_x}(y - \gamma), \tag{23a}$$

$$\dot{y} = \frac{1}{\tau_y}[\alpha(y - y^3) - x]. \tag{23b}$$

In order to develop an understanding for the way that such a model can simulate the rapid D-O warmings, followed by slow coolings, we ~~shall discuss~~ start by discussing its autonomous behavior, for time-independent γ~~, first. Next, we shall give a~~

425   ~~physical meaning to the variables in the climate context and introduce time-dependent forcing exerted by a background state~~ ~~via $\gamma = \gamma(t)$~~.
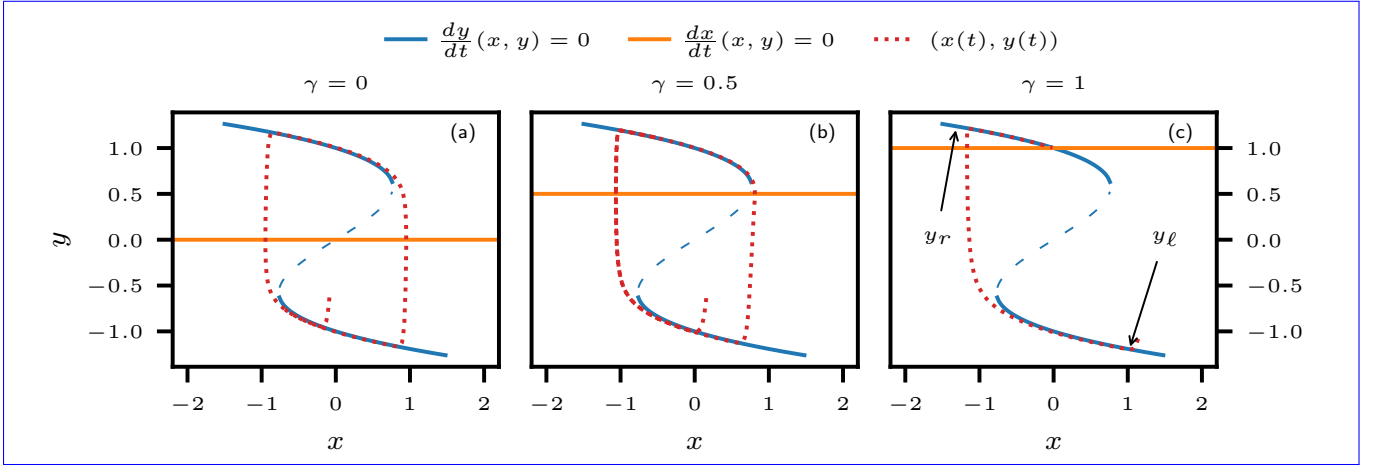
20

Figure 9. Nullclines of the autonomous FHN model governed by Eqs. (23) with large time scale separation, for $\alpha = 2, \tau_x = 100$ and $\tau_y = 10$; the nullclines of the fast y-component are in blue and of the slow x-component in orange. (a–c) One illustrative trajectory (red dotted) for $\gamma = 0, 0.5$, and 1.0, respectively. The upper branch and the lower branch (solid blue) correspond to the roots y_r and y_ℓ, respectively, as defined in the text. For fixed values of x, they constitute stable fixed points for Eq. (23b). The middle branch (dashed blue) corresponds to the unstable fixed point for Eq. (23b) for a given x. The trajectories for panels (a) and (b) follow a limit cycle, since the x-nullcline does not intersect with either of the *stable branches* of the y-nullcline, given that $|\gamma| < \sqrt{1/3}$, while the trajectory in panel (c) approaches a single stable fixed point for the coupled system, formed by the intersection of the x-nullcline with the y_ℓ branch of the y-nullcline.

~~Consider~~ First, consider the case of large time scale separation

$$\tau_x \underset{\sim}{>>} \gg \tau_y. \tag{24}$$

This choice guarantees that the fast y-component adjusts adiabatically to quasi-static changes of the slow x-component. The
430   time derivative of $y(t)$, as shown in Fig. 10(a), exhibits either three real roots or a single one, depending on the value of $x(t)$, which shifts the graph of the cubic polynomial $P_3(x,y) = \alpha(y - y^3) - x$ globally upwards or downwards. Of the three potential roots, the outer two are stable fixed points for $y(t)$ at a fixed value of x, while the inner one is unstable. Note that the two stable fixed points are always located either left or right of the local minimum or maximum of $P_3(x,y)$, respectively. Accordingly, we label them y_ℓ and y_r. ~~Thus, the~~ The positions of the local extrema, namely $y_{\min} = -\sqrt{1/3}$ and $y_{\max} = \sqrt{1/3}$, provide an
435   upper and a lower bound for the left and right stable fixed point, respectively.

~~Given the large time scale separation, the y-component will be close to either one of the two stable fixed points for a given~~ Now, let us investigate the coupled dynamics of the slow and fast variables $x(t)$ and $y(t)$. Assume we are in a state where $x > 2\alpha/\sqrt{27}$ such that y_ℓ is the only root of $P_3(x,y)$. Provided that $|\gamma| < \sqrt{1/3}$, the time derivative $\dot{x}$ and x ~~; hence, $y(t)$ must be outside the interval spanned by the two local extrema: $y(t) \notin (-\sqrt{1/3}, \sqrt{1/3})$. In the overall evolution of the~~
440   ~~solution, though, the stable fixed point that momentarily attracts $y(t)$ is destabilized by~~ itself will have opposite signs, with the consequence that a slow adjustment ~~of $x(t)$,~~ process of $x(t)$ sets in. This will shift the polynomial $P_3(x,y)$ upwards in panel (a)
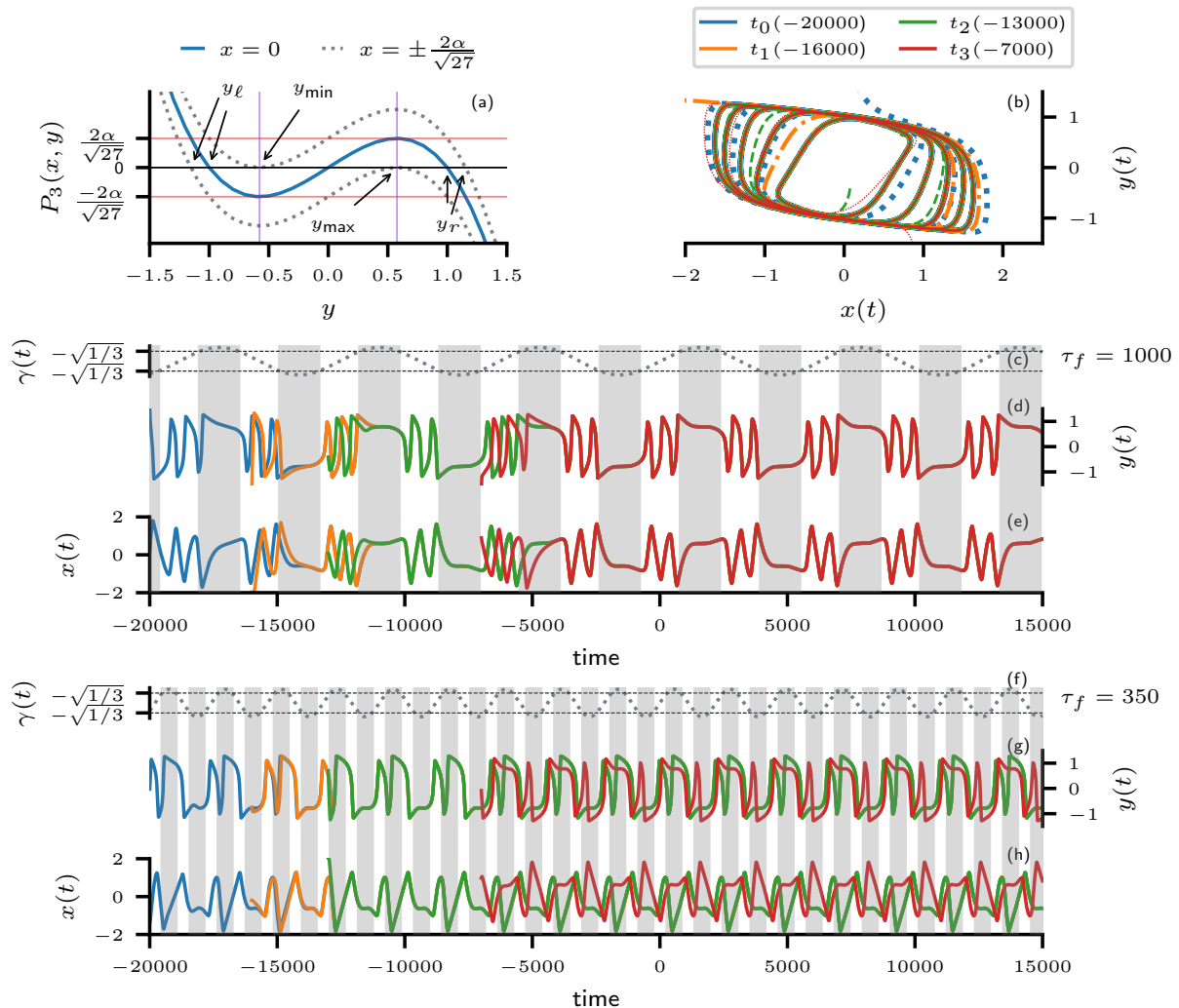
21

Figure 10. FitzHugh-Nagumo (FHN) model with ~~time scales $\tau_f = 2000$,~~ parameters $\tau_x = 100$, $\tau_y = 60$, and $\alpha = 2$. (a) The cubic ~~term~~ polynomial $P_3(x,y)$ of the fast derivative ~~$P_3(x,y)$~~ as a function of y for $x=0$ (solid blue line); ~~dashed~~ the red lines point to the local maximal and minimal values of $P_3(x,y)$, namely $\pm 2a/\sqrt{27}$, respectively — these are the maximal values by which P_3 can be shifted up or down, while maintaining all of its three roots; the dotted gray lines indicate the ~~same~~ shifted function with $x=\pm 2\alpha/\sqrt{27}$. The purple lines labeled y_{min} and y_{max} mark the right and left boundaries for the roots y_ℓ and y_r, respectively: y_ℓ and y_r can never be located in between the two purple lines. (b) Trajectories of the nonautonomous model ~~, with $\gamma(t) = \sin(t/\tau_f)$,~~ $\gamma(t) = 0.8\sin(t/\tau_f)$ and ~~starting at the times $\{t_0 = -20\,\text{kyr}, t_1 = -16\,\text{kyr}, t_2 = -13\,\text{kyr}, t_3 = -7\,\text{kyr}\}$ $\tau_f = 1\,000$,~~ plotted in the (x,y) ~~plane, using different colors for t_0, t_1, t_2~~ phase plane; the trajectories are colored by their starting times $\{t_0 = -20\,\text{kyr}, t_1 = -16\,\text{kyr}, t_2 = -13\,\text{kyr}, t_3 = -7\,\text{kyr}\}$ and ~~t_3~~ the initial positions were drawn from a standard Gaussian bivariate distribution. (c) The slow time-dependent forcing ~~$\gamma = \gamma(t)$~~ $\gamma(t) = \sin(t/1\,000)$. (d, e) The same trajectories as in (b), but plotted in time ~~,~~ as $y = y(t)$ and $x = x(t)$, respectively ~~.~~; ~~in panels (e–h)~~ ~~Same as panels (ec–e)~~, but for the fast time-dependent forcing $\gamma(t) = \sin(t/350)$. The gray shading in panels (c)–(h) indicates intervals during which $|\gamma| > \sqrt{1/3}$ and the internal oscillation is ~~hence~~ suppressed.

of Fig. 10 which in turn revives the other two roots of $P_3(x,y)$. The fast $y(t)$ closely follows y_ℓ, which is shifted accordingly. Once $x(t) = -2\alpha/\sqrt{27}$, the root y_ℓ stops existing and a fast transition to the neighborhood of the opposite ~~stable fixed point~~ root y_r ensues. This transition switches the sign of $\dot{x}(t)$ and the slow adjustment of $x(t)$ now happens in the opposite direction.

In the (x,y)-plane, this behavior manifests itself as a stable limit cycle. However, any value $|\gamma| > \sqrt{1/3}$ prevents $\dot{x}(t)$ from switching sign and therefore interrupts the cyclic destruction and revival of the ~~opposite fixed points for $y(t)$~~respective opposite root of $P_3(x,y)$. Instead, $|\gamma| > \sqrt{1/3}$ gives rise to a single stable fixed point for the entire system in the (x,y)-plane and, in this case, both variables relax towards ~~this equilibrium~~it.

In fact, in the autonomous setting, the system's qualitative behavior is ~~ultimately~~ controlled by the value of the parameter γ, which decides between internal oscillations along a limit cycle and relaxation towards a fixed point in the (x,y)-plane. ~~This~~ Note that previously we referred to the roots y_ℓ and y_r also as stable fixed points of y for a given value of x. Here, the term *stable fixed point* refers to the entire system defined by the coupled ODEs (23a) and (23b). Both $\gamma = \pm\sqrt{1/3}$ are critical values of γ that give rise to supercritical Hopf bifurcations of the coupled system's fixed points; recall Fig. 4 of Sect. 2.1.

This behavior can be better understood by considering the nullclines of (23b) and (23a) in the (x,y)-plane, as shown in Fig. 9. If the branches of the y-nullcline that correspond to y_ℓ and y_r, and thus to stable fixed points of (23b) for a given value of x, intersect with the x-nullcline given by $y = \gamma$, then this intersection constitutes a stable fixed point for the entire system.

If they do not, the system first relaxes along the fast direction toward the y-nullcline. Only then the adjustment of the slow component starts to drag the system along the y-nullcline in the direction where the distance to the x-nullcline decreases. At the point where the y-nullcline reverses, the fast component is immediately attracted by the other branch of the fast nullcline and the same process starts all over again.

So far we have described the formation of the limit cycle in the FHN model under the assumption of clear time scale separation and the independence of the x-nullcline $\{y = \gamma\}$ from x. See Rocsoreanu et al. (2012) for the emergence of the limit cycle in the more general FHN model.

The highly nonlinear, two-time behavior of the FHN model modifies somewhat the ~~general appearance of~~ way that stable limit cycles ~~via Hopf bifurcation whose normal form~~, arise in it. While we saw the oscillation's radius grow with the square root of the bifurcation parameter in the case of the normal form given by Eqs. (3–5), ~~was discussed in Sec. 2.1~~ in the case of the FHN model, the radius of the oscillations actually grows exponentially over a small range of γ-values right after the bifurcation point and then stabilizes. These exponentially growing stable limit cycles have been termed "canard cycles" (Benoît, 1983). Roberts and Saha (2017) have pointed out a possible link between canard cycles and D-O cycles and they play a role in other excitable climate models; see Pierini and Ghil (2021, and references therein).

A pullback attractor of a periodically forced FHN model. Introducing a sinusoidal time dependence

$$\gamma \rightarrow \gamma(t) \underset{=}{\propto} \sin(t/\tau_{\mathrm{f}}) \tag{25}$$

into the slow equation (23a) makes the system nonautonomous, as discussed in general terms in ~~See~~Sect. 3.2, and it periodically switches the self-oscillatory behavior on and off. We consider here the case in which the variations of the external forcing

23

475 $\gamma(t; \tau_\mathrm{f})$ ~~varies slowly with respect to all~~ occur on a slower time scale than the entire internal dynamics, i.e.,

$$\tau_\mathrm{f} > \geq \tau_x > \geq \tau_y. \tag{26}$$

Note that we give up here on the restriction of strict time scale separation between $x(t)$ and $y(t)$, as expressed by Eq. (24).

   The trajectories plotted in Figs. 10(~~b~~c)–(e) ~~represent, in fact,~~ and (f)–(h) represent the solutions of such a periodically forced FHN model starting at different points in the past~~on an arbitrary time axis~~. The time units are arbitrary and the two sets of
480 solutions are for two different forcing time scales τ_f. These trajectories illustrate the applicability of the pullback perspective suggested by ~~Sec~~Sect. 3.2 and Fig. 6 to the periodically forced FHN model. In contrast to the ~~previous examples~~ illustrative examples of Sect. 3.2, an analytical solution is not available in this case. However, this small sample of numerically computed trajectories, together with the phenomenological discussion herein, is quite sufficient for an intuitive understanding of the system's pullback behavior.

485 ~~Most strikingly, the trajectory t_1 that starts at $-16\,000$ during a nonoscillatory time interval is immediately synchronized to the trajectory t_0 that started even earlier, at $-20\,000$. The other two trajectories both start during intervals when internal oscillations are supported and maintain their individual phase throughout the oscillatory interval. It takes a breakdown of the limit cycles~~ For panels (c)–(e) of Fig. 10, the forcing's time scale is much slower then the internal time scales. The amplitude of the forcing $\gamma(t)$ was chosen such that it repeatedly crosses the two thresholds $\pm\sqrt{1/3}$ and thus induces a sequence
490 of Hopf bifurcations by switching between intervals of self-sustained oscillation and attraction to a ~~common~~ stable fixed point~~for these trajectories to synchronize to the "older" trajectories . Here, synchronization means thatthey can visually~~. Crossing such a bifurcation point due to slow changes in the forcing is referred to as a bifurcation-induced tipping or *B-tipping* (Ashwin et al., 2012; Ghil, 2019; Ghil and Lucarini, 2020).

   Strikingly, all trajectories converge to one another during non-oscillatory time intervals, when they are simultaneously
495 attracted by the single existing fixed point. During oscillatory intervals, phase differences between individual trajectories may, in principle, persist. Still, convergence during a single non-oscillatory interval is so strong that, after it, the trajectories can no longer be ~~distinguished; numerically~~discriminated visually. Numerically, however, the distance between trajectories only tends to zero but never reaches it. At the end of non-oscillatory intervals, the trajectories reenter the oscillatory regime always from the same location in the (x, y)-plane — to within negligible numerical differences — and, hence, very nearly repeat themselves.
500 Qualitatively speaking, the PBA $\mathscr{A}$ — i.e., the family of invariant snapshots $\{\mathcal{A}(t)\}_{t \in \mathbb{R}}$ of Eq. (14) — is an infinite repetition of the common trajectory structure that can be observed in Figs. 10(d,e) between $-5\,000$ and $15\,000$ time units. In the case at hand, each snapshot $\mathcal{A}(t)$ consists of a single point.

   ~~The model trajectories ' behavior in the figure can be explained, in greater detail, as follows: whenever $|\gamma(t)| > \sqrt{1/3}$, all trajectories are attracted by a single point~~ For panels (f)–(h) of Fig. 10, the time scale separation between the forcing and
505 the internal dynamics is reduced, resulting in a qualitatively different behavior of the nonautonomous system. The frequency of occurrence of B-tipping points is much higher, and hence the trajectories do not even execute a full oscillation during a single time interval that permits oscillations. As a result, two stable patterns of trajectories are formed. These two patterns

can be brought into agreement by switching the sign of one pattern and shifting it in time by $\tau_f/2$. This symmetry reflects the symmetry of the stable nullcline of the fast system component as shown in Fig. 9.

Again, the PBA of this nonautonomous system can be thought of as an infinite repetition of the common trajectory structure that can be observed in Figs. 10(g,h) between $-5\,000$ and $15\,000$ time units. In contrast to the slow-forcing case, each snapshot $\mathcal{A}(t)$ now is comprised of two points in the (x,y)-plane~~; hence — given~~. This example illustrates how the action of an external force on an autonomous system can give rise to considerably richer dynamics, which crucially depends on both the system's ~~intrinsic dynamics being fast with respect to the forcing, cf.~~ internal variability and the nature of the forcing.

A random attractor of a periodically and stochastically forced FHN model. Based on the brief introduction to RDSs in Sect. 3.2, we take our investigation of the periodically forced FHN model one step further and include a random component into the external forcing, acting on the model's fast y-component:

$$\mathrm{d}x = \frac{1}{\tau_x}(y - \gamma(t))\mathrm{d}t, \tag{27a}$$

$$\mathrm{d}y = \frac{1}{\tau_y}[\alpha(y - y^3) - x]\mathrm{d}t + \sigma \mathrm{d}\eta. \tag{27b}$$

Here, η denotes a Wiener process, as in Eq. (21) — ~~during a single nonoscillatory time interval, all trajectories are strongly bundled by the fixed point and can no longer be discriminated visually. This bundling guarantees that the distance between different trajectories becomes arbitrarily small after only afew nonoscillatory intervals. Furthermore, the system's fixed point during the nonoscillatory behavior is fully determined by~~ i.e., a continuous stochastic process whose increments $\mathrm{d}\eta$ are independently and normally distributed, with mean zero and unit variance — and $\gamma(t)$ ~~; therefore, at the end of such an interval, the system reenters the oscillatory regime always from the same location in the (x,y)-plane and, therewith, the trajectories very nearly repeat themselves. Qualitatively speaking, the PBA $\mathscr{A}$~~ remains a periodic forcing of the x-component proportional to $\sin(\tau_f t)$.

In order to study the random attractor of this system, we compute trajectories with random initial conditions over a time span long enough to reveal the asymptotic behavior, as shown in Fig. 11. For both the slower and the faster deterministic forcing — ~~or, according to Eq.~~ i.e., $\tau_f = 1\,000$ and $\tau_f = 350$, as studied in the previous paragraphs — several random attractors are approximated for increasing noise variance values σ in Eq. (27b). For each attractor approximation, we use 20 trajectories with the same noise realization. Each random attractor (red) is shown together with the corresponding PBA of the FHN system subject to purely periodic forcing (blue and green).

For the long-periodic forcing with $\tau_f = 1\,000$, the ~~family of invariant snapshots $\{\mathcal{A}(t)\}_{t\in\mathbb{R}}$ — is an infinite repetition of the common trajectory structure that can be observed in Figs. 10(d, e) between 0 and 10 000.~~ trajectories in Fig. 11(a) converge fairly rapidly to a single one, as in the case with no noise in Figs. 10(d,e). Furthermore, there is a clear similarity of pattern and proximity in phase between the PBA of the deterministic system and the random attractor. However, the deviations of the random attractor from the PBA increase in both pattern and phase as the noise variance increases. These deviations are most striking during the oscillatory intervals, because the noise can induce phase shifts in the oscillations, which then persist for
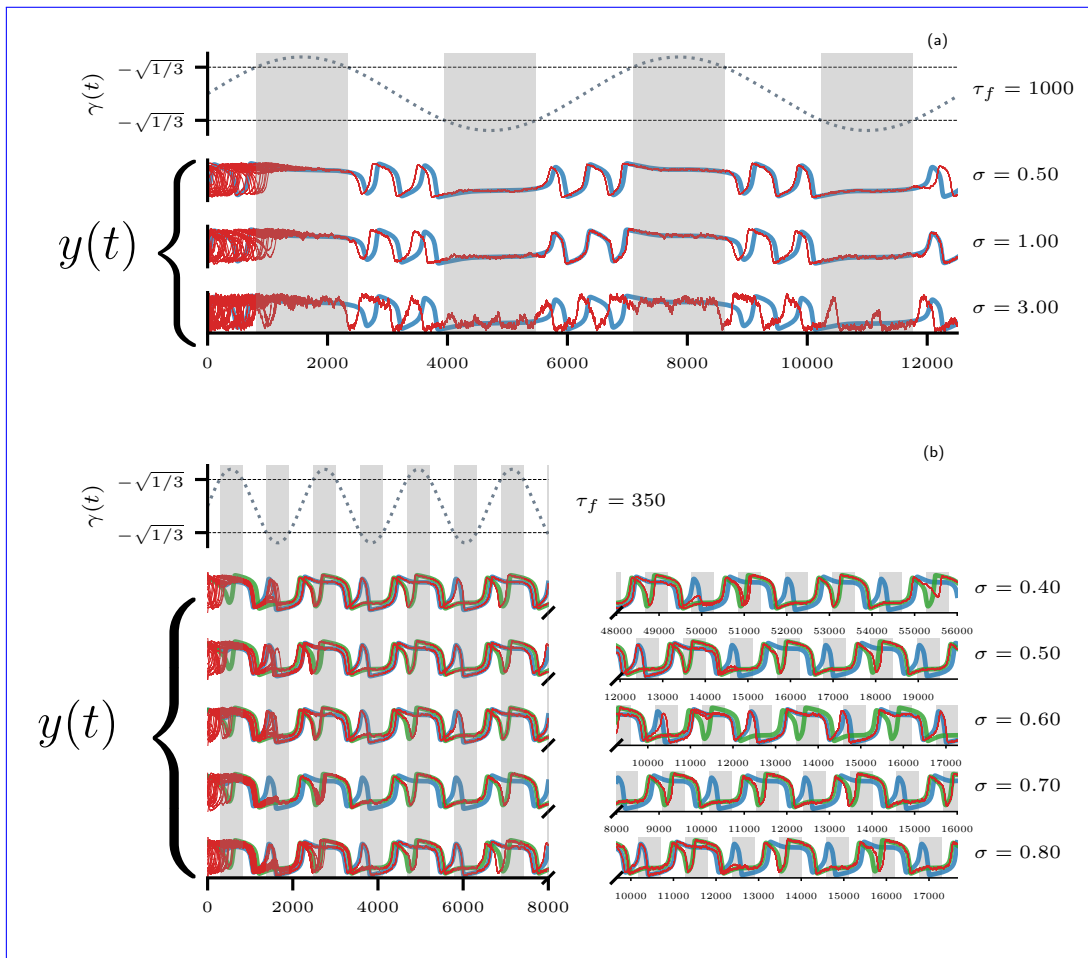
Figure 11. Random attractor of the periodically and stochastically forced FHN model governed by Eqs. (27). (a) Results for slow periodic forcing with period $\tau_f = 1\,000$. The top graph shows the periodic forcing, with non-oscillatory intervals marked by gray shading. The next three graphs show the fast y-component of the approximate random attractors, as per Eq. (27b); the noise variance σ increases from top to bottom. Each random attractor (solid red) is approximated by integrating 20 trajectories with different initial conditions over time and using the same Wiener process as their common stochastic forcing; the corresponding deterministic PBA is shown in blue. The random attractors and the PBA are very similar for small noise variances, but they differ more and more as the noise variance increases. (b) Results for faster periodic forcing with period $\tau_f = 350$. The forcing is only shown for the first 8000 time units, with non-oscillatory intervals again shaded gray. The left part of panel (b) shows 5 approximate random attractors, computed as in panel (a), on a common time axis. The panel's right part shows their continuations on individual time axis in order to display the moment when full noise-induced synchronization of the trajectories takes place. Prior to this point, the random attractor is split into two branches, which closely follow the PBA of the deterministic system (blue and green). For $\sigma = 0.7$, the synchronization takes place already during the first 8 000 time units.

540   the duration of the oscillatory interval. During non-oscillatory intervals, the random attractor is less susceptible to the noise, because the resulting perturbations decay in the presence of a stable fixed point of the underlying deterministic system.

For the shorter-period forcing with $\tau_f = 350$, the PBA of the deterministic system features two stable branches, which could in principle persist in the random attractor. As for the case of $\tau_f = 1\,000$, a rapid convergence of the trajectories can be observed for all noise variances. However, two separate bundles of trajectories persist, each associated with one of the two separate branches of the deterministic PBA. Only after some time do the two bundles merge and subsequently follow either one of the two branches of the PBA or the other. This phenomenon is called *noise-induced synchronization* (e.g., Arnold, 1988; Chekroun et al., 2011). Which of the two PBA branches the random attractor follows depends on the exact noise realization. The random attractor may also switch irregularly from one branch of the PBA to the other (not shown). Already in the simple setup explored here, one notices that the higher the noise variance, the faster the synchronization of the trajectories. This statement must be understood probabilistically: it may certainly happen for two given noise realizations that the random attractor with the higher noise level takes longer to synchronize, as is the case for $\sigma = 0.7$ and $\sigma = 0.8$ in Fig. 11(b).

The investigation carried out herein assesses a very special case of an FHN model's random attractor. Random attractors of FHN-type models have been studied intensively (e.g., Wang, 2009; Yamakou et al., 2019). Most studies so far, however, have concentrated on the excitable regime of the stochastically forced FHN model, i.e., the deterministic model's parameters were chosen so as to exhibit a single stable fixed point in the absence of the noise. The noise variance was then chosen sufficiently high to ensure that random fluctuations can push the system out of equilibrium and allow it to take a round trip on what would be the deterministic model's limit cycle, given different parameter values. The situation studied here is rather different, as shown across Figs. 9–11.

An FHN model of the NGRIP record. Readers who are familiar with the NGRIP δ^{18}O record (North Greenland Ice Core Project members, 2004) might have realized already the qualitative resemblance between the proxy data and the fast component's trajectory of the periodically forced FHN model in Fig. 10(d). In particular, the prominent sawtooth pattern of the data is satisfactorily captured by the ~~fast-slow~~ fast–slow dynamics of the model.

Figure 12 shows a trajectory of the FHN model for which the sinusoidal forcing used in Fig. 10 was replaced by a rescaled time series of atmospheric CO_2 concentrations retrieved from Antarctic ice cores (Bereiter et al., 2015):

$$\gamma(t) \propto CO_2(t). \tag{28}$$

Is it remarkable how well this simple forcing brings the oscillatory intervals of the FHN model into agreement with the time intervals of the record that are dominated by D-O cycles, without any systematic tuning of the model parameters. Clearly, the CO_2-forced FHN model fails to reproduce the exact waiting times between D-O events. However, with these waiting times being at least in part stochastically determined (Ditlevsen et al., 2007), the purely deterministic FHN model is not meant to reproduce the exact pattern of D-O events. Vettoretti et al. (under review) have carried out a detailed study on the use of a CO_2-forced FHN model to simulate D-O variability.

In fact, ~~Rousseau et al. (2022, Fig. 6)~~ Rousseau et al. (2022, Fig. 6) describe in detail a somewhat more complex, proxy record-based picture of the interaction between D-O event-rich episodes, ~~Heinrich (1988)~~ (Heinrich, 1988) events, and longer-
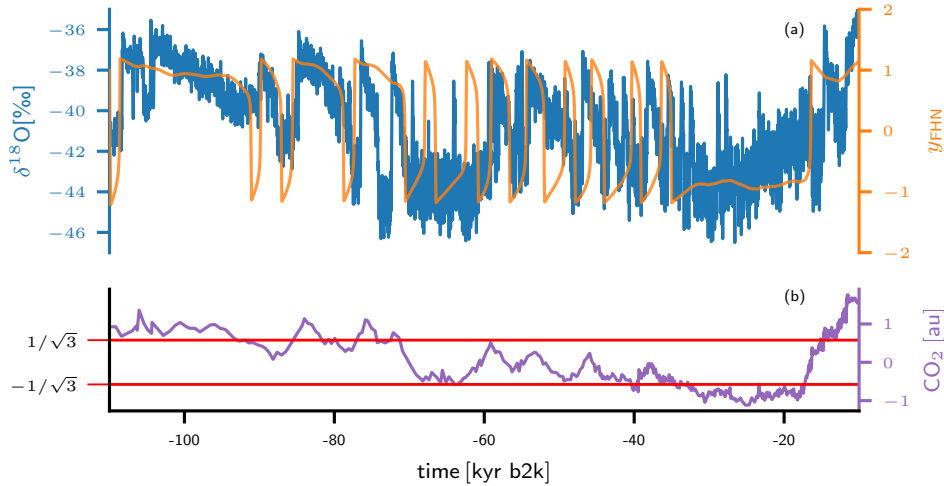
Figure 12. FHN model fit to the NGRIP δ^{18}O data. (a) Fast component $y_{\mathrm{FHN}}(t)$ of an FHN model forced with historical CO_2 concentrations (orange) together with the observed δ^{18}O record (blue) from the NGRIP ice core (Seierstad et al., 2014). (b) Rescaled atmospheric CO_2 concentrations from Antarctic ice cores in arbitrary units (au) (Bereiter et al., 2015); the horizontal red lines indicate the upper and lower bounds, $y_{\min} = -\sqrt{1/3}$ and $y_{\max} = \sqrt{1/3}$, of the free-oscillation regime.

term cooling trends. It is quite possible that a simple model like the one in this section but including explicitly continental ice sheets could capture such a detailed picture.

In the present framework, the FHN model's fast variable $y(t)$ may be interpreted as the intensity of the Atlantic Meridional Overturning Circulation (AMOC), which switches between on and off states during self-oscillatory behavior; see, for instance, Henry et al. (2016), Ghil (1994, Table 5) and Ghil and Lucarini (2020, Table I). The slower x-variable that drives the transition between the on and off states of the AMOC may then be taken, for instance, as the waxing and waning of northern hemisphere ice sheets ~~(e.g., Ghil et al., 1987)~~(e.g., Ghil et al., 1987), linked in turn to varying ice shelf extent ~~(e.g., Boers et al., 2018)~~(e.g., Boers et al., 2018) or as the weakening and strengthening of Antarctic bottom water production (Vettoretti et al., under review).

The interaction between the fast variable and the slow one happens here in the presence of a climate forcing represented by CO_2 concentration. On the much slower time scales of Quaternary glaciations, an interplay between the CO_2 concentration and mean global temperature might also occur, as we shall see in the next section.

4   AN NDS FOR THE QUATERNARY GLACIATIONS

Apparently, it is Crucifix (2013) who first applied pullback ideas to the problems of Quaternary glaciations, independently of earlier work on the topic in the climate literature (Ghil et al., 2008; Chekroun et al., 2011; Bódai and Tél, 2012). His work

The concepts and tools summarized in Sec. 3.2 could shed further light on several problems not quite yet solved concerning Quaternary glaciations and paleoclimate in general. A short and highly incomplete list of the interesting problems that might gain by such a treatment is the following:

1. What are the causes of the MPT and what is the part of intrinsic climate variability and that of the orbital forcing therein? See discussion in Sec. 2.2.

2. What causes the large continuous backgound of the observed spectrum: is it deterministic chaos, stochastic forcing or both? See discussion of Fig. 4.

3. Particularly complex problems are associated with Heinrich and D-O events and their modulation over longer time intervals by orbital forcing and other slow-acting changes in atmospheric composition, geology, ocean circulation, and so on. See, for instance, Rousseau et al. (2021, and references therein).

4. It is well established by now that a snowball mode occurred several times in Earth's geologic history, but we still know fairly little about how the planet got into, and especially out of, such a mode (e.g., Pierrehumbert,2004).

Box 2. Some open questions concerning Quaternary glaciations.

590   concentrated mainly on the connection between the pacemaking role of the orbital forcing and the observed irregularity of the glacial terminations during the late Pleistocene, cf. Broecker and Van Donk (1970) and Ghil and Childress (1987, Fig. 11.2).

Based on the considerable success of NDS and RDS applications to other climate problems — such as ENSO (Ghil et al., 2008; Ghil and Zaliapin, 2015; Chekroun et al., 2018; Marangio et al., 2019), the wind-driven ocean circulation (Pierini et al., 2016, 2018) or the evaluation of the ensemble simulations routinely performed in support of the Assessment Reports of the

595   Intergovernmental Panel on Climate Change (Drótos et al., 2015; Vissio et al., 2020) — it would appear worthwhile to proceed further along these lines.

Box 2 summarizes open questions with respect to Quarternary glaciations whose investigation should be aided by NDS and RDS theory. Of course, each of these problems requires one or more distinct climate models, as well as very careful modeling of the kinds of time-dependent changes in forcing and parameters that are most enlightening, as well as most relevant and

600   plausible. A good way would be to start testing ideas with relatively simple models and pursue the investigation systematically across a hierarchy of models — through intermediate ones and on to the most detailed ones — in order to further increase understanding of the climate system and of its predictability on the various paleoclimatic time scales mentioned in the list above.

Such an approach can usefully complement the more common one of merely pushing onwards to higher and higher model

605   resolution in order to achieve ever more detailed simulations of the system's behavior for a limited set of semi-empirical parameter values. Ghil (2001) and Held (2005), among others, have emphasized the need to pursue such a model hierarchy, as originally proposed by ~~Schneider and Dickinson (1974)~~Schneider and Dickinson (1974), in order to balance the need
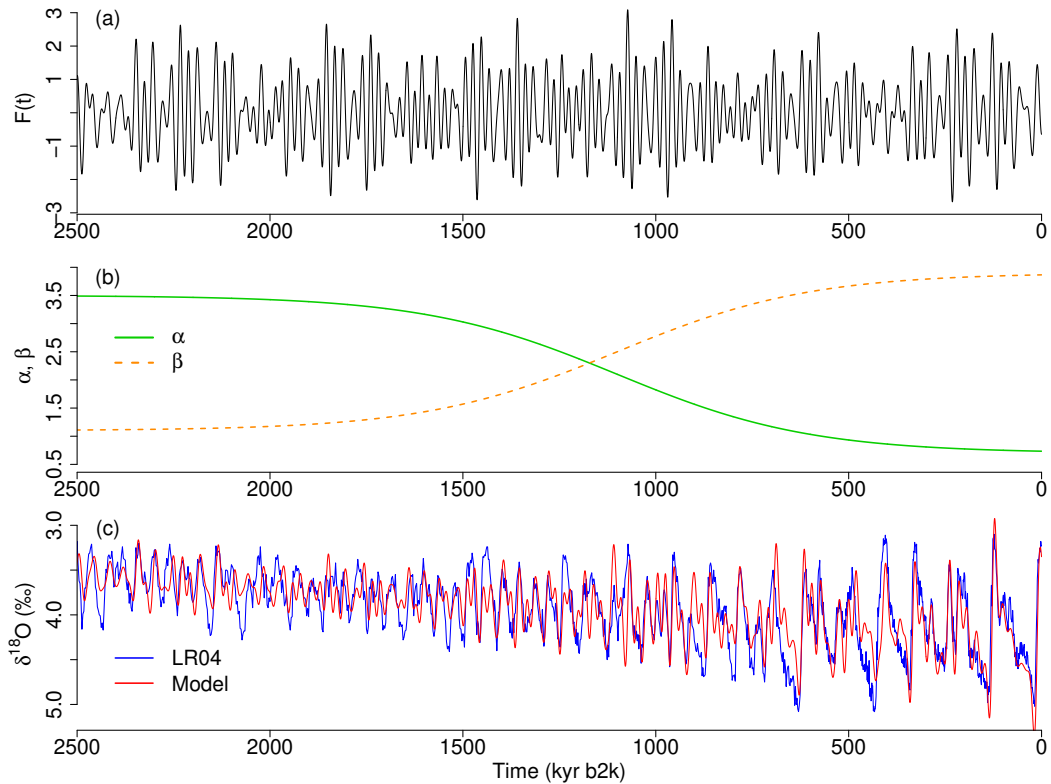
29

Figure 13. Glacial-interglacial cycles simulated by the modified Daruka and Ditlevsen model of Eqs. (29, 31): (a) June 21 insolation $F(t)$ at 65°N, normalized to have mean zero and unit standard deviation over the last 1 000 kyr. (b) Slowly changing parameters $\alpha(t)$ and $\beta(t)$ introduced to give rise to the MPT. (c) Simulated glacial-interglacial cycles $\delta^{18}O_{model}$ (red) in comparison with the benthic $\delta^{18}O$ (blue).

to broaden the number of plausible hypotheses vs the need for confronting them with spatio-temporal details derived from observations.

610   In this section, we illustrate how the PBA concept can help shed more light upon the dynamics of ice age models. ~~For this purpose, we apply the Daruka and Ditlevsen (2016) model of glacial-interglacial cycles with slight modifications. We show first that this model approximates rather well the glacial cycles inferred from~~ As pointed out in Sect. 3.1 and elsewhere in this paper, there is a long history of modeling the climate of the Quaternary by means of conceptual models, and many nonautonomous models have been proposed to simulate glacial-interglacial cycles of the last 400 kyr to 2.6 Myr, based on the orbital forcing. In

615   Appendix A, we provide a long but still not exhaustive list of glacial-cycle models and specify some of their key characteristics, including the degree of their success at simulating the MPT; see also the discussion in Sect. 2.2.

     Among these glacial-cycle models, the model of Daruka and Ditlevsen (2016, DD16 hereafter) belongs to the more abstract ones, as it is not derived from detailed physical considerations. Still, its concise form, interesting nonlinear dynamics, and ability to simulate glacial cycles, as well as the MPT, make the DD16 model well suited for our illustrative purposes. We

620   first slightly modify this model from its original formulation. We do so mainly in order for the model to better approximate

the benthic δ^{18}O proxy reconstruction of ~~Lisiecki and Raymo (2005) and then compute the model's PBA~~ glacial–interglacial cycles due to Lisiecki and Raymo (2005), especially the timing of glacial terminations; compare our Fig. 13 with Fig. 1 in DD16. Thereafter, we compute the PBAs of the modified DD16 model, M-DD16 hereafter, to investigate the dynamical stability of its glacial cycles over the past 2.6 Myr.

625   ~~The~~ Our model's variables, following DD16, are a global temperature anomaly y that is proportional to minus the global ice volume and an effective climatic memory term x that represents the internal degrees of freedom. In the deterministic case, the governing equations of the M-DD16 model are given by

$$\tau\dot{x} = \lambda y, \tag{29a}$$

$$\tau\dot{y} = -\alpha(t) + x - x^3 - \beta(t)F(t)x - \kappa y; \tag{29b}$$

630 here t is the time in kyr and $F(t)$ is the normalized June 21 insolation at 65°N, based on the calculations of Laskar et al. (2004), as shown in Fig. 13(a). The constant parameter values are chosen as $\kappa = 1$, $\tau = 100$, and $\lambda = 10$. Note that — with this choice of λ and unlike in the FHN model of D–O oscillations in Sect. 3.3 — x is the fast variable and y is the slow one.

~~The equations generalize a first-order ODE system that is equivalent to the Duffing form of the nonlinear-spring equation discussed in Sec. 2.2. The use of such simple forms of first-order systems in paleoclimate models was initiated by Saltzman et al. (1981)~~

635 ~~.We deviate from Daruka and Ditlevsen (2016), though, by introducing~~ In the original DD16 model, MPT-like behavior was produced by a slow sigmoid variation of the parameter κ in Eq. (29b),

$$\kappa(t) = \kappa_1 + 0.5(\kappa_0 - \kappa_1)\left(1.0 - \tanh\left(\frac{t - t_0}{t_s}\right)\right). \tag{30}$$

In our M-DD16 model, we introduce instead a slow change in the parameters ~~$\alpha(t)$ and $\beta(t)$~~ $\alpha(t)$ and $\beta(t)$ of Eq. (29b), as follows:

640 $$\alpha(t) = 2.1 - 1.4\tanh\left((t + 1100)/500\right), \tag{31a}$$

$$\beta(t) = 2.5 + 1.4\tanh\left((t + 1100)/500\right). \tag{31b}$$

The functions ~~$\alpha(t)$ and $\beta(t)$~~ $\alpha(t)$ and $\beta(t)$ so defined are plotted in Fig. 13(b) and they induce, as we shall see forthwith, a change in model behavior that not only resembles the MPT but also shows correct timings for most of the terminations. Moreover, to simulate δ^{18}O$_{\text{model}}$, we add a ~~slow~~ linear trend to the slow variable y to mimic the overall cooling at time scales of

645 millions of years, thus: $\delta^{18}\text{O}_{\text{model}} = 4.3 - 1.4y + 0.0003t$. Equations (29) generalize a first-order ODE system that is equivalent to the Duffing form of the nonlinear-spring equation (7) discussed in Sect. 2.2. The use of such classical first-order systems — like the Duffing and Van der Pol ones — in paleoclimate models was initiated by Saltzman et al. (1981); see also Sect. 2.2 herein.

     Figure 13(c) shows a time series of simulated ~~glacial-interglacial~~ glacial–interglacial changes $\delta^{18}\text{O}_{\text{model}}$ (red) in comparison

650 with the benthic δ^{18}O (blue) of Lisiecki and Raymo (2005). The model's initial condition is taken to be $x = -1$ and $y = 0$ at ~~$t = -10\,000$ kyr~~ $t = 10\,000$ kyr b2k and, since the insolation forcing in panel (a) is prescribed as a time series with 100-yr

sampling, we solved Eq. (29) using Heun's predictor-corrector method (Isaacson and Keller, 2012, Ch. 8) with a step size of 100 yr. A large spin up time is chosen to guarantee that transient effects caused by the initial conditions have abated by the year 2.6 Ma b2k, which is the starting point for the time interval under study. The correlation between the model simulation and the proxy record is 0.75 for the time interval from ~~−2 600~~ 2 600 kyr to 0 kyr b2k, and 0.72 over the interval from ~~−1 000~~ 1 000 kyr to 0 kyr b2k. Varying the parameters slowly across the time interval of interest, as shown in Fig. 13(b), leads to a change in the frequency — from a dominant 41-kyr periodicity prior to the MPT, at roughly 1.2 Ma kyr b2k, to a dominant 100-kyr periodicity after the MPT, at roughly 800 kyr b2k — and a substantial increase in the amplitude.
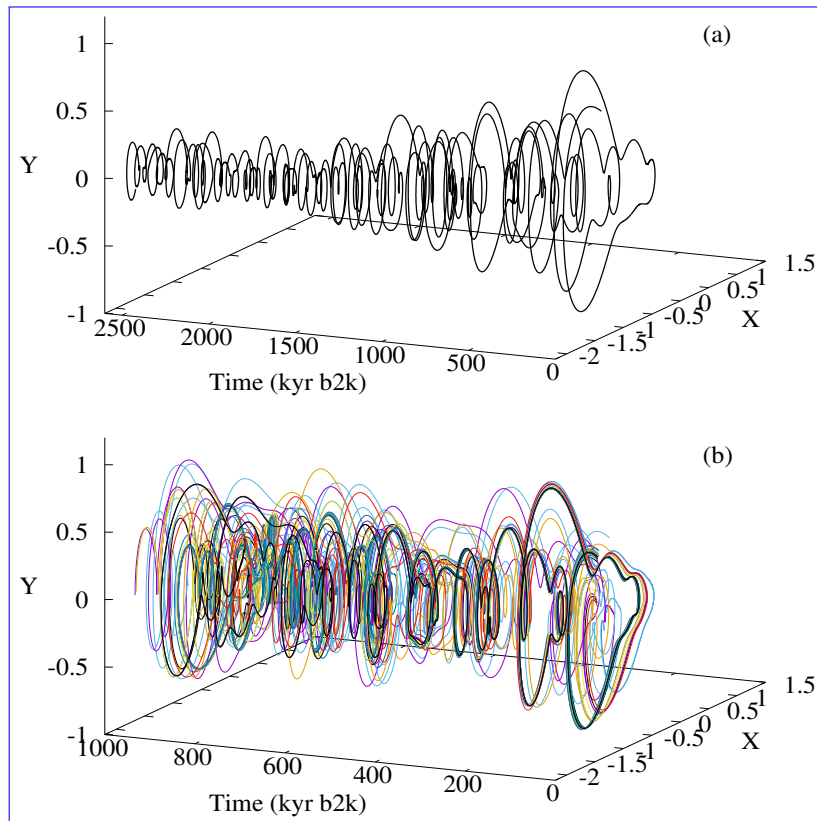
Figure 14. PBA of the ~~modified Daruka and Ditlevsen (2016)~~ M-DD16 model ~~given~~ governed by Eqs. (29), approximated by forty trajectories starting from random initial conditions in $(x, y) \in [-2, 2] \times [-2, 2]$ at $t = -10\,000$ kyr. (a) The ~~behavior~~ PBA corresponding to Fig. 13, with the slowly changing parameters $\alpha(t)$ and $\beta(t)$ given by Eqs. (31); and (b) the ~~behavior~~ PBA for $\alpha(t)$ and $\beta(t)$ kept constant at the post-MPT values of $\alpha = 0.7$ and $\beta = 3.9$. In panel (b), the PBA is shown over a shorter time interval of the last 1 000 kyr so that the detailed structure is more clearly visible. Without changes in α and β in time, the overall structure of the PBA is similar before and after 1 000 kyr b2k.

We next approximate the PBA by taking 40 random initial conditions at 10 ~~Myr~~ Ma b2k and integrating the model of Eqs. (29, 31) up to the present time. The PBA in this case is simply a moving fixed point, as plotted in Fig. 14(a), since the

model dynamics is predominantly stable in the long time interval prior to the MPT~~that is situated around 1.2–0.8 Myr b2k~~. It would appear, therewith, that the orbital forcing simply moves this fixed point around and fully determines Earth's climate. This agrees with the clear statement in DD16 that "First and foremost, our model does not have any internal periods of oscillation."

However, when keeping the parameters α and β fixed at their post-MPT values $\alpha = 0.7$ and $\beta = 3.9$ throughout the simulation interval and repeating the computation of the PBA, a more complex picture arises. In the latter case, Fig. 14(b) shows a bunching of trajectories into separate fuzzy clusters, subject to the quasi-periodic orbital forcing of Fig. 13(a).

There are two interesting inferences to be drawn. First, post-MPT dynamics is much more irregular and unstable than the ~~stable, quasi-periodic~~ more stable dynamics prior to the MPT. ~~This result is consistent with Mitsui et al. (2015), who showed the~~ The robustness of the 40-kyr glacial cycles and instability of 100-kyr glacial cycles against perturbations ~~in terms of mode-locking theory and strange nonchaotic attractors~~is in line with the conclusions of previous studies (Mitsui et al., 2015; Quinn et al., 20 . It also appears to be consistent with the ~~Willeit et al. (2019)~~ Willeit et al. (2019) simulation of the last 3 Myr of Earth history that used an Earth System Model of Intermediate Complexity (CLIMBER-2) that included ice sheets and a carbon cycle, along with ~~atmosphere-ocean variables~~atmosphere–ocean dynamics. In their work, trajectories starting from different initial states tended to converge to a single attracting trajectory in the Early Pleistocene, while several distinct trajectories survived in the Late Pleistocene after the MPT.

Second, the separate bundles or "ropes" of trajectories in Fig. 14(b) seem to point to the type of *generalized synchronization* discussed in the paleoclimate context by ~~De Saedeleer et al. (2013)~~ De Saedeleer et al. (2013) and in the context of interannual and interdecadal climate variability by Pierini and Ghil (2021) and ~~Vannitsem et al. (2021)~~Vannitsem et al. (2021). Generalized synchronization in the strict sense of the existence of a map between a time-dependent control and the system's asymptotic behavior has only been shown to hold for nonchaotic systems. Work is under way, though, to further generalize this concept to chaotic systems as well (e.g., Rulkov et al., 1995; Zhang et al., 2007).

5   Conclusions

In this review-and-research paper, we have covered in ~~See~~Sect. 1 the contributions of the 1970s to the rebirth of the Milankovitch (1920) theory of the ice ages and in ~~See~~Sect. 2 the 1980s advances in modeling the Quaternary climate's intrinsic variability. In ~~See~~Sect. 3, we presented first results on the ~~interaction between~~ effects of the orbital insolation forcing of ~~See~~Sect. 1 ~~and~~ on the intrinsic variability of ~~See~~Sect. 2, and proceeded to introduce the novel concepts and tools of the theory of nonautonomous and random dynamical systems (NDSs and RDSs) that can help to better model and understand ~~this interaction~~these effects. The section concluded by the formulation and study of a FitzHugh-Nagumo (FHN)-type model of recurrent Dansgaard-Oeschger (D-O) events, in which historical CO_2 concentrations induced episodes of D-O events alternating with episodes of their absence, in excellent qualitative agreement with NGRIP $\delta^{18}O$ data; see again Fig. 12.

Finally, in ~~See~~Sect. 4, we listed a number of open issues on Quaternary and longer paleoclimate time scales, and proposed to address them by using the tools of ~~See~~Sect. 3.2. This approach was illustrated by a Duffing-type model of Daruka and Ditlevsen

(2016), modified to include slow changes in the parameters that mimic such changes in the Earth system over the duration of the Quaternary period.

695   When the parameters are gradually changed in time so as to exhibit the mid-Pleistocene transition (MPT), the PBA is simply a moving fixed point. However, when the parameters are fixed at their post-MPT values, the PBA so obtained is chaotic and exhibits clusters of trajectories that we termed *ropes*. This suggests (a) that the stability of the system is gradually lost while crossing the MPT; and (b) that Late Pleistocene climate, albeit chaotic, may well be subject to a kind of generalized synchronization (cf. De Saedeleer et al., 2013; Pierini and Ghil, 2021; Vannitsem et al., 2021) with the orbital forcing that

700 is illustrated in Fig. 5 of ~~See~~Sect. 3.1 herein. In the specific situation at hand, separate ropes may be associated with various combination tones of the forcing frequencies.

    In a broader perspective — and leaving aside various finer points of the MPT conversation outlined in ~~See~~Sect. 2.2 — one can see the work that was reviewed and extended in this paper as a confirmation of the fine intuition of Emiliani and Geiss (1959), six decades ago, as summarized in and further expanded by ~~Ghil and Childress (1987, Sec. 12, pp. 446-447)~~

705 Ghil and Childress (1987, Sect. 12, pp. 446-447):

    "Hence the following scenario (compare Emiliani and Geiss, 1959) suggests itself for the successive climatic transitions from Pliocene to Pleistocene and from Early to Late Pleistocene: As land masses moved towards more northerly positions, small ice caps formed on mountain chains and at high latitudes. These ice caps, due to their feedback on albedo, made climate more sensitive to insolation variations than it was in the total absence of ice. The response of the climatic system to such variations

710 during the Early Pleistocene (2 000 [kyr]–1 000 [kyr] ago) was still relatively weak, of a fraction of a degree centigrade in global temperature perhaps, in agreement with the quasi-equilibrium results of ~~Section~~ Sect. 10.2.

    As ice caps passed, about 1 000 [kyr] ago, a certain critical size, the unforced system jumped from its stable equilibrium to its stable limit-cycle state (Figures 12.5 and 12.9), increasing dramatically the climate's total variability, to a few degrees centigrade in global temperature. Furthermore, resonant response became possible (see also Oerlemans (1984) [in

715 ~~Berger et al. (1984)~~Berger et al. (1984)] and ~~Sergin (1979)~~Sergin (1979)), enhancing abruptly the amplitude of the peak at 100 ~~kyr~~kyr, among others."

    The take-home message is that slow and fast processes, both intrinsic and extrinsic, interact on all paleoclimatic time scales and that we are mastering the art of modeling such interactions.

Video supplement. The video supplement to this article illustrates the pullback attractor (PBA) associated with the simple system governed by Eqs. (16) and (17). It shows a heat map of the phase plane, derived from an increasing number of trajectories with common initial time $t_i = -200$ and final time $t_f = 200$. The initial radius and phase of each trajectory are randomly sampled from Gaussian distributions centered at $\mu_\rho = 20$ and $\mu_\phi = 0$ with standard deviations of $\sigma_\rho = 5$ and $\sigma_\phi = 10$, respectively. Over the course of the video, 100 trajectories are continuously added to the heat map and the annular disc

$$\mathcal{D} = \{(\rho, \phi) : \rho \in [\mu - \alpha\beta, \mu + \alpha\beta] \text{ and } \phi \in [0, 2\pi)\} \tag{32}$$

fills up. The heat map in Fig. 6(b) is a snapshot from this video at time $t = 0.2$.

Appendix A: Low-order dynamical-system models of glacial cycles

The dynamical modeling of glacial cycles dates back to the 1970s. Calder (1974) proposed a model of global ice volume changes that had different sensitivities to the insolation when ice sheets were waxing and waning, respectively. His model can be written as an NDS, according to Paillard (2001). Subsequently, conceptual dynamical models were further developed (e.g., Imbrie and Imbrie, 1980; Berger, 1999). Some of the more recent models simulate the proxy records of glacial cycles remarkably well (Paillard, 1998; Imbrie et al., 2011; Parrenin and Paillard, 2012).

Shortly after Calder (1974) presented his work, Weertman (1976) proposed a simple ice-sheet model based on the flow law of a perfectly plastic solid. Next, researchers extended this simple ice sheet model by coupling it with an energy-balance model (Källén et al., 1979) and further with the isostatic response of the underlying bedrock (Oerlemans, 1980; Ghil and Le Treut, 1981; Le Treut . Källén et al. (1979) found self-sustained oscillations in their simple coupled ice sheet–energy balance model. Le Treut and Ghil (1983) showed that the dominant 100-kyr periodicity of glacial cycles is generated — in their simple oscillator coupling ice sheet volume with the bedrock's isostatic rebound, on the one hand, and with the atmosphere and ocean's energy balance, on the other — via nonlinear resonance with the multi-periodic orbital forcing. More recently, Verbitsky et al. (2018) developed a simple physical model through a scaling argument that respects the underlying physics. Another branch of simple models explicitly includes the carbon cycle as an essential ingredient (Saltzman and Maasch, 1990; Paillard and Parrenin, 2004; Hogg, 2008; Toggweiler, 20

A deeper understanding of glaciation cycles cannot be obtained without process-based models that focus on the detailed physics and biogeochemical phenomena involved (Berger et al., 1999; Ganopolski and Calov, 2011; Abe-Ouchi et al., 2013; Ganopolski a . Still, simple dynamical models like the ones mentioned above, as well as models based on more mathematical considerations, are useful, too, for understanding the climate system's behavior and changes therein, since complex systems can sometimes exhibit familiar dynamics, regardless of the details (Nicolis and Nicolis, 2012; Crucifix, 2011). As Henri Poincaré pointed out, "mathematics is the art of giving the same name to different things."

For example, coupled nonlinear oscillators frequently exhibit synchronization with simple frequency ratios, either with each other (Pikovsky et al., 2001) or with the forcing (Ghil and Childress, 1987). Thus, mathematical models that ignore many physical details may also help us elucidate emergent properties in paleoclimatic dynamics (Tziperman et al., 2006; Crucifix, 2011, 2012; De

Author(s) (year)	Succint description	Dynamical properties	Is the Middle-Pleistocene Transition (MPT)-like behavior generated?	Additional comments
Low-order dynamical systems models of glacial cycles				
Calder (1974)	Model of the global ice volume with different sensitivities to the insolation during growth and retreat, respectively.	Nonchaotic. No self-sustained oscillation in the absence of forcing	Not specifically addressed	His model can be written as a non-autonomous dynamical system (NDS) (Paillard, 2001)
Weertman (1976)	Simplified ice sheet model based on the flow law of a perfectly plastic solid	Nonchaotic. No self-sustained oscillation in the absence of forcing	Not specifically addressed	
Källén et al. (1979) Ghil and Le Treut (1981) Le Treut and Ghil (1983) Ghil (1994)	Ice sheet–bedrock–temperature coupled oscillator; see the text for details	Chaotic in the presence of orbital forcing (Ghil, 1994). Exhibits self-sustained oscillations with a period of ≈ 10 kyr; the basic mechanism for getting ~ 100-kyr cycle is nonlinear resonance at a difference tone between the 19-kyr and 23-kyr precession cycles (Le Treut and Ghil, 1983); see Sect. 2.1 herein.	Not explicitly. It can exhibit, however, the MPT in principle, since 41-kyr oscillations as well as dominant 100-kyr oscillations can be generated, depending on the model's parameter values.	Källén et al. (1979) is an ice sheet–temperature coupled oscillator. Ghil and Le Treut (1981) introduced the bedrock and Le Treut and Ghil (1983) added the orbital forcing.
Imbrie and Imbrie (1980)	Piecewise-linear model with two different time scales for ice sheet waxing and wanning	Nonchaotic. No self-sustained oscillation in the absence of forcing	Not specifically addressed	400-kyr periodicity is more dominant than 100-kyr periodicity.
Saltzman and Maasch (1988) Saltzman and Maasch (1990) Maasch and Saltzman (1990)	Coupled oscillator based on ice–CO_2–ocean temperature (or NADW) coupling. Nonlinearlity is only in the CO_2 component.	Nonchaotic. After the MPT, it exhibits self-sustained oscillations with a period of ~ 100 kyr in the absence of forcing.	Yes, the MPT arises via a Hopf bifurcation in the underlying system; see also Crucifix (2012).	It has a strange nonchaotic attractor, as well as a chaotic one, depending on the parameter setting (Mitsui and Aihara, 2014).
Paillard (1998) Parrenin and Paillard (2003) Parrenin and Paillard (2012)	Hybrid dynamical system with discrete states that switch when conditions are satisfied	Nonchaotic but the dynamics is sensitive to parameter changes near the switching boundaries (Paillard, 2001). No self-sustained oscillations in the absense of forcing.	Yes, in Paillard (1998)	The authors call these models *relaxation oscillators*, in spite of their discrete-state formulation.
Berger (1999)	Delayed differential equation for ice volume	Robustness of trajectories against random perturbations is mentioned. It exhibits damped oscillations in the absence of forcing.	Not specifically addressed.	
Paillard and Parrenin (2004)	Coupled oscillator based on Northern hemisphere ice volume–Antarctic ice extent–CO_2 coupling.	Nonchaotic. It exhibits self-sustained oscillations in the absence of forcing.	Yes, the MPT is induced by a slow drift in the bottom water formation efficiency around the Antarctic	Ashwin et al. (2018) showed that this model can exhibit chaotic dynamics when it is slightly modified.
Ashkenazy and Tziperman (2004) Tziperman et al. (2006)	An ice mass model, which simplifies the sea-ice switch model of Gildor and Tziperman (2000)	It exhibits self-sustained oscillations in the absence of forcing. Nonchaotic under the orbital forcing.	Yes, in Ashkenazy and Tziperman (2004), where the maximum ice volume threshold is increased in time according to the result	Uses the temperature-precipitation feedback introduced by Källén et al. (1979).

Author(s) (year)	Succint description	Dynamical properties	Is the Middle-Pleistocene Transition (MPT)-like behavior generated?	Additional comments
Low-order dynamical systems models of glacial cycles				
Huybers (2007) Huybers (2011)	The ice mass grows monotonically and collapses to zero when it exceeds a threshold modulated by the obliquity (Huybers, 2007) or by a hybrid measure consisting of the obliquity and climatic precession (Huybers, 2011).	It exhibits self-sustained oscillations in the absence of forcing; nonchaotic.	Yes, in Huybers (2007)	
Imbrie et al. (2011)	Data-based, phase-space model for Pleistocene ice volume with thresholds.	Due to the presence of the threshold, the model is sensitive to changes in parameters or in its position in phase space.	Yes, MPT-like behavior is produced solely by changes in orbital parameters.	
Crucifix (2012) De Saedeleer et al. (2013)	Forced Van der Pol (VdP) oscillator model; closely related to the FHN model used in Sect. 3.3 herein.	Nonchaotic (Crucifix, 2012) but sensitive to the noise; see Additional Comment. It exhibits self-sustained oscillations in the absence of forcing.	Yes, MPT-like behavior is generated via a Hopf bifurcation with an explosive character (Crucifix, 2012)	Ashwin et al. (2018) showed that this model has only a small parameter region corresponding to chaotic dynamics, but may have a wider chaotic region when it is generalized to the VdP-Duffing system.
Mitsui et al. (2015)	One-dimensional phase oscillator model	Nonchaotic	Yes, MPT-like frequency change accompanies a smooth or nonsmooth saddle-node bifurcation of tori.	It has a strange nonchaotic attractor or a quasiperiodic attractor in a classical sense, i.e., not in the pullback sense.
Ashwin and Ditlevsen (2015)	Two-dimensional forced limit cycle oscillator	Nonchaotic; overall stability of simulated glacial cycles against dynamical noise is reported.	It exhibits MPT-like behavior via a transcritical bifurcation of the slow manifold in the fast dynamics.	
Omta et al. (2016)	Forced two-dimensional oscillator consisting of ocean alkalinity and calcifier population	Nonchaotic or chaotic given periodic forcing, depending on the parameters. It exhibits self-sustained oscillations in the absence of forcing.	Yes	
Daruka and Ditlevsen (2016)	Forced Duffing oscillator–type model.	No self-sustained oscillations in the absence of forcing. Can be chaotic depending on parameter values; the authors call this the "climatic butterfly effect."	Yes, MPT-like behavior is induced by a slow change in the damping coefficient parameter κ.	See also Sect. 4 herein.
Huybers and Langmuir (2017)	Coupled system of ice volume, temperature and atmospheric CO_2, incorporating a delayed CO_2 contribution from ocean ridge volcanism. It is reduced to a forced 1-D delay differential equation	A phase-locking property is reported. The underlying system has two stable and one unstable stationary states. However, it $_{37}$ close to a Hopf bifurcation point and is excitable by the forcing.	Yes, the MPT is modeled as a switch from small-amplitude oscillations to large-amplitude ones, which is triggered by the amplitude modulation of obliquity cycles.	

Author(s) (year)	Succint description	Dynamical properties	Is the Middle-Pleistocene Transition (MPT)-like behavior generated?	Additional comments
Low-order dynamical systems models of glacial cycles				
Quinn et al. (2017)	Scalar delay-differential equation for ice volume, derived from the Saltzman and Maasch (1988) model, via the linear chain approximation.	Nonchaotic before the MPT and temporarily chaotic after the MPT around 800 kyr b2k. In the absence of astronomical forcing, the delayed feedback leads to bistable behavior, in which stable large-amplitude oscillations and an equilibrium coexist.	Yes, MPT-like behavior is induced by summer insolation forcing as a transition from small-amplitude ~41-kyr cycles to large-amplitude ~100-kyr cycles.	
Ashwin et al. (2018)	Study of several low-order dynamical systems models, including Paillard and Parrenin (2004), Crucifix (2012) and a generalized VdP-Duffing oscillator.	Chaotic or nonchaotic depending on the model and its parameter values.	Not explicitly discussed. The models can, however, exhibit MPT-like behavior in principle, because 41-kyr oscillations as well as dominant 100-kyr oscillations are generated depending on parameter values.	The authors stress the possibility of chaotic dynamics occurring.
Verbitsky et al. (2018)	Coupled model relying on ice-sheet basal temperature–ocean temperature coupling, deduced from physical laws via a scaling analysis.	Nonchaotic. No self-sustained oscillations in the absence of forcing. The 100-kyr cycles are attributed to a period-doubling response to 41-kyr obliquity cycles.	Yes, MPT-like behavior is induced by an enhancement of positive feedbacks against negative feedbacks in the model.	
Talento and Ganopolski (2021)	Ice volume–CO_2 coupled conceptual model		Not specifically addressed.	This model was developed to simulate the last 800-kyr of glacial cycles and Earth's future climate on the Myr time scale.
Low-order dynamical models in which stochastic processes are of the essence				
Benzi et al. (1981, 1982) Nicolis (1981)	Two independent formulations of a stochastic-resonance model. Additive noise favors the bimodal response of a periodically modified double-well potential to global annual insolation variations	Additive stochastic perturbations play a key role	Not specifically addressed. An MPT-llike transition could be obtained by subjecting both the depth of the deterministic double well and the pure periodicity of its modulation to a more or les gradual modification.	Benzi et al. (1981, 1982) and Nicolis (1981) proposed the stochastic-resonance idea for ice-age cyclicity, independently of each other.
Matteucci (1989)	Generalized stochastic resonance model with obliquity and precessional forcing	Additive stochastic perturbations play a key role.	Not specifically addressed.	
Pelletier (2003)	Model based on the coherence resonance mechanism (Pikovsky and Kurths, 1997) uses a single temperature ODE with a discrete delay.	Additive stochastic perturbations play a key role.	Yes	The delay feedback in the temperature is based on ice sheet extent reconstructions and affects the model's albedo.
Ditlevsen (2010)	Generalized stochastic resonance model with obliquity and precessional forcing	Additive stochastic perturbations play a key role.	Yes	The model has an underlying bifurcation structure following Paillard (1998) .

or test different orbital hypotheses (Huybers, 2011). Many low-order models of glacial dynamics are listed in Tab. A1, although it is by no means exhaustive.

Appendix B: PBA for a limit cycle with sinusoidally modulated radius

Here we study the system of two formally decoupled ODEs

$$\frac{d\rho}{dt} = \alpha(\mu + \beta\sin(\nu t) - \rho), \quad \frac{d\phi}{dt} = \omega \qquad \text{with} \qquad \rho > 0,\, \mu > 0 \tag{B1}$$

760   that was introduced in ~~See~~Sect. 3.2 and analytically derive its invariant sets

$$\mathcal{A}(t) = \{ \big(\alpha\beta\sin(\nu t + \vartheta) + \mu, \varphi\big) : \varphi \in [0, 2\pi) \} \qquad \forall t \in \mathbb{R}, \tag{B2}$$

as well as the corresponding pullback attractor (PBA). Following ~~Crauel and Kloeden (2015)~~Crauel and Kloeden (2015), the PBA is given by the family

$$\mathscr{A} = \{\mathcal{A}\}_{t:t\in\mathbb{R}} \tag{B3}$$

765   First, we define $\Delta\rho(t) = \rho(t) - \mu$, which gives rise to

$$\frac{\mathrm{d}\Delta\rho(t)}{\mathrm{d}t} = -\alpha\Delta\rho(t) + \alpha\beta\sin(\nu t). \tag{B4}$$

This is an inhomogeneous ODE and can thus be solved by the variation of parameters method (e.g., Boyce and DiPrima, 2005). The Ansatz

$$\Delta\rho(t) = c(t)\, e^{-\alpha(t-t_0)} \tag{B5}$$

770   yields

$$\frac{\mathrm{d}\Delta\rho(t)}{\mathrm{d}t} = -\alpha\Delta\rho(t) + \frac{\mathrm{d}c(t)}{\mathrm{d}t}\, e^{-\alpha(t-t_0)}. \tag{B6}$$

A comparison with Eq. (B4) requires

$$\frac{\mathrm{d}}{\mathrm{d}t}c(t) = \alpha\beta\sin(\nu t)e^{+\alpha(t-t_0)}, \tag{B7}$$

and hence

775    $$c(t) = \int_{t_0}^{t} \alpha\beta\sin(\nu t')e^{+\alpha(t'-t_0)}\mathrm{d}t' + \gamma = [\alpha\beta\sin(\nu t')\frac{1}{\alpha}e^{+\alpha(t'-t_0)}]_{t_0}^{t} - \int_{t_0}^{t} \frac{\nu}{\alpha}\alpha\beta\cos(\nu t')e^{+\alpha(t'-t_0)}\mathrm{d}t' + \gamma. \tag{B8}$$

Repeated partial integration yields

$$\int_{t_0}^{t} \frac{\nu}{\alpha}\alpha\beta\cos(\nu t')e^{+\alpha(t'-t_0)}\mathrm{d}t' = [\frac{\nu}{\alpha}\alpha\beta\cos(\nu t')\frac{1}{\alpha}e^{+\alpha(t'-t_0)}]_{t_0}^{t} + \int_{t_0}^{t} \frac{\nu^2}{\alpha^2}\alpha\beta\sin(\nu t')e^{+\alpha(t'-t_0)}\mathrm{d}t'. \tag{B9}$$

Therefore, we find

$$(1+\frac{\nu^2}{\alpha^2})\int_{t_0}^{t}\alpha\beta\sin(\nu t')e^{+\alpha(t'-t_0)}\mathrm{d}t' = [\alpha\beta\sin(\nu t')\frac{1}{\alpha}e^{+\alpha(t'-t_0)}]_{t_0}^{t} - [\frac{\nu}{\alpha}\alpha\beta\cos(\nu t')\frac{1}{\alpha}e^{+\alpha(t'-t_0)}]_{t_0}^{t} \tag{B10}$$

and finally

$$c(t) = \frac{1}{(1+\frac{\nu^2}{\alpha^2})}\left(\underbrace{[\beta\sin(\nu t')e^{+\alpha(t'-t_0)}]_{t_0}^{t}}_{=\beta[\sin(\nu t)e^{\alpha(t-t_0)}-\sin(\nu t_0)]} - \underbrace{[\frac{\nu\beta}{\alpha}\cos(\nu t')e^{+\alpha(t'-t_0)}]_{t_0}^{t}}_{=\frac{\nu\beta}{\alpha}[\cos(\nu t)e^{\alpha(t-t_0)}-\cos(\nu t_0)]} +\gamma\right). \tag{B11}$$

Plugging this result into the Ansatz (B5) yields

$$\Delta\rho(t,t_0) = \frac{1}{(1+\frac{\nu^2}{\alpha^2})}\left(\beta[\sin(\nu t)-\sin(\nu t_0)e^{-\alpha(t-t_0)}] - \frac{\nu\beta}{\alpha}[\cos(\nu t)-\cos(\nu t_0)e^{-\alpha(t-t_0)}]\right) + \gamma e^{-\alpha(t-t_0)}, \tag{B12}$$

with the initial conditions

$$\Delta\rho(t_0,t_0) = \gamma. \tag{B13}$$

In the pullback limit, all the terms that carry a factor $e^{-\alpha(t-t_0)}$ vanish and thus

$$\lim_{t_0\to-\infty}\Delta\rho(t,t_0) = \frac{1}{(1+\frac{\nu^2}{\alpha^2})}\left(\beta\sin(\nu t) - \frac{\nu\beta}{\alpha}\cos(\nu t)\right) = \alpha\beta\sin(\nu t+\vartheta), \tag{B14}$$

with $\vartheta = \arctan(-\nu/\alpha)$. For comparison, the modulation of the target radius itself was given by $\beta\sin(\nu t)$ and hence it is amplified by the factor of α. Since ρ is restricted to positive values, this solution requires $\alpha\beta < \mu$.

Since the evolution in time of the phase $\phi(t)$ is trivial, different initial conditions for the phase do not converge. Hence, the time-dependent sets that are invariant with respect to the dynamics of the system are

$$\mathcal{A}(t) = \{(\rho(t),\phi) : \phi \in [0,2\pi)\} = \{(\alpha\beta\sin(\nu t+\vartheta),\phi) : \phi \in [0,2\pi)\}. \tag{B15}$$

Defined as the indexed family of all $\mathcal{A}(t)$, the system's PBA is comprised of the family of circles

$$\mathscr{A} = \{A(t)\}_{t\in\mathbb{R}} = \{(\alpha\beta\sin(\nu t+\vartheta),\phi) : \phi \in [0,2\pi)\}_{t\in\mathbb{R}}. \tag{B16}$$

800

References

Abe-Ouchi, A., Saito, F., Kawamura, K., Raymo, M. E., Okuno, J., Takahashi, K., and Blatter, H.: Insolation-driven 100,000-year glacial cycles and hysteresis of ice-sheet volume, Nature, 500, 190–193, https://doi.org/10.1038/nature12374, 2013.

Arnold, L.: Random Dynamical Systems, Springer, New York, 1988.

Arnold, V. I.: Geometrical Methods in the Theory of Ordinary Differential Equations, Springer Science & Business Media; first Russian edition 1978, 2012.

Ashkenazy, Y. and Tziperman, E.: Are the 41 kyr glacial oscillations a linear response to Milankovitch forcing?, Quaternary Science Reviews, 23, 1879–1890, https://doi.org/10.1016/j.quascirev.2004.04.008, 2004.

Ashwin, P. and Ditlevsen, P.: The middle Pleistocene transition as a generic bifurcation on a slow manifold, Climate Dynamics, 45, 2683–2695, 2015.

Ashwin, P., Wieczorek, S., Vitolo, R., and Cox, P.: Tipping points in open systems: bifurcation, noise-induced and rate-dependent examples in the climate system, Philosophical Transactions of the Royal Society A: Mathematical, Physical and Engineering Sciences, 370, 1166–1184, 2012.

Ashwin, P., David Camp, C., and von der Heydt, A. S.: Chaotic and non-chaotic response to quasiperiodic forcing: limits to predictability of ice ages paced by Milankovitch forcing, Dynamics and Statistics of the Climate System, 3, 1–20, https://doi.org/10.1093/climsys/dzy002, 2018.

Bagniewski, W., Ghil, M., and Rousseau, D. D.: Automatic detection of abrupt transitions in paleoclimate records, Chaos: An Interdisciplinary Journal of Nonlinear Science, 31, 113 129, https://doi.org/10.1063/5.0062543, 2021.

Barenblatt, G. I.: Scaling, Self-Similarity, and Intermediate Asymptotics, Cambridge University Press, 1996.

Benoît, É.: Systèmes lents-rapides dans R^3 et leurs canards, Astérisque, pp. 109–110, 1983.

Benzi, R., Sutera, A., and Vulpiani, A.: The mechanism of stochastic resonance, Journal of Physics A: mathematical and general, 14, L453, 1981.

Benzi, R., Parisi, G., Sutera, A., and Vulpiani, A.: Stochastic resonance in climatic change, Tellus, 34, 10–15, https://doi.org/10.3402/tellusa.v34i1.10782, 1982.

Bereiter, B., Eggleston, S., Schmitt, J., Nehrbass-Ahles, C., Stocker, T. F., Fischer, H., Kipfstuhl, S., and Chappellaz, J.: Revision of the EPICA Dome C CO2 record from 800 to 600 kyr before present, Geophysical Research Letters, 42, 542–549, 2015.

Berger, A.: Long-term variations of daily insolation and Quaternary climatic changes, Journal of the Atmospheric Sciences, 35, 2362–2367, 1978.

Berger, A., Imbrie, J., Hays, J., Kukla, G., and Saltzman, B., eds.: Milankovitch and Climate: Understanding the Response to Astronomical Forcing, vols. I & II, D. Reidel Publ. Co., Dordrecht/Boston, reissued in 2013 by Springer Science & Business Media, 1984.

Berger, A., Li, X., and Loutre, M.-F.: Modelling northern hemisphere ice volume over the last 3 Ma, Quaternary Science Reviews, 18, 1–11, 1999.

Berger, W. H.: The 100-kyr ice-age cycle: Internal oscillation or inclinational forcing?, International Journal of Earth Sciences, 88, 305–316, https://doi.org/10.1007/s005310050266, 1999.

Bódai, T. and Tél, T.: Annual variability in a conceptual climate model: Snapshot attractors, hysteresis in extreme events, and climate sensitivity, Chaos: An Interdisciplinary Journal of Nonlinear Science, 22, 023110, https://doi.org/http://dx.doi.org/10.1063/1.3697984, 2012.

Bódai, T., Lucarini, V., Lunkeit, F., and Boschi, R.: Global instability in the Ghil-Sellers model, Climate Dynamics, 44, 3361–3381, 2015.

Boers, N., Chekroun, M. D., Liu, H., Kondrashov, D., Rousseau, D.-D., Svensson, A., Bigler, M., and Ghil, M.: Inverse stochastic–dynamic models for high-resolution Greenland ice core records, Earth System Dynamics, 8, 1171–1190, https://doi.org/10.5194/esd-8-1171-2017, 2017a.

Boers, N., Goswami, B., and Ghil, M.: A complete representation of uncertainties in layer-counted paleoclimatic archives, Climate of the Past, 13, 1169–1180, https://doi.org/10.5194/cp-13-1169-2017, 2017b.

Boers, N., Ghil, M., and Rousseau, D.-D.: Ocean circulation, ice shelf, and sea ice interactions explain Dansgaard–Oeschger cycles, Proceedings of the National Academy of Sciences, 115, E11 005–E11 014, https://doi.org/10.1073/pnas.1802573115, 2018.

Bond, G., Showers, W., Cheseby, M., Peter Almasi, R. L., deMenocal, P., Priore, P., Irka Hajdas, H. C., and Bonani, G.: A pervasive millennial-scale cycle in North Atlantic Holocene and glacial climates, Science, 278, 1257–1266, https://doi.org/10.1126/science.278.5341.1257, 1997.

Boyce, W. E. and DiPrima, R. C.: Elementary Differential Equations and Boundary Value Problems, 8th Edition, John Wiley & Sons, 2005.

Broecker, W. S. and Van Donk, J.: Insolation changes, ice volumes, and the O^{18} record in deep-sea cores, Reviews of Geophysics, 8, 169–198, 1970.

Budyko, M. I.: The effect of solar radiation variations on the climate of the Earth, Tellus, 21, 611–619, 1969.

Calder, N.: Arithmetic of ice ages, Nature, 252, 216–218, https://doi.org/https://doi.org/10.1038/252216a0, 1974.

Caraballo, T. and Han, X.: Applied Nonautonomous and Random Dynamical Systems: Applied Dynamical Systems, Springer Science + Business Media, 2017.

Charó, G. D., Chekroun, M. D., Sciamarella, D., and Ghil, M.: Noise-driven topological changes in chaotic dynamics, arXiv:2010.09611v7 [nlin.CD], 2021.

Chekroun, M. D., Simonnet, E., and Ghil, M.: Stochastic climate dynamics: random attractors and time-dependent invariant measures, Physica D: Nonlinear Phenomena, 240, 1685–1700, https://doi.org/10.1016/j.physd.2011.06.005, 2011.

Chekroun, M. D., Ghil, M., and Neelin, J. D.: Pullback attractor crisis in a delay differential ENSO model, in: Advances in Nonlinear Geosciences, edited by Tsonis, A. A., pp. 1–33, Springer Science & Business Media, https://doi.org/10.1007/978-3-319-58895-7, 2018.

Crafoord, C. and Källén, E.: A note on the condition for existence of more than one steady state solution in Budyko-Sellers type models, J. Atmos. Sci, 35, 1123–1125, 1978.

Crauel, H. and Kloeden, P. E.: Nonautonomous and random attractors, Jahresbericht der Deutschen Mathematiker-Vereinigung, 117, 173–206, 2015.

Crucifix, M.: How can a glacial inception be predicted?, The Holocene, 21, 831–842, 2011.

Crucifix, M.: Oscillators and relaxation phenomena in Pleistocene climate theory, Philosophical Transactions of the Royal Society A: Mathematical, Physical and Engineering Sciences, 370, 1140–1165, 2012.

Crucifix, M.: Why could ice ages be unpredictable?, Clim. Past, 9, 2253–2267, 2013.

Dansgaard, W., Johnsen, S. J., Clausen, H. B., Dahl-Jensen, D., Gundestrup, N. S., Hammer, C. U., Hvidberg, C. S., Steffensen, J. P., Sveinbjörnsdottir, A. E., Jouzel, J., and Bond, G.: Evidence for general instability of past climate from a 250-kyr ice-core record, Nature, 364, 218–220, https://doi.org/10.1038/364218a0, 1993.

Daruka, I. and Ditlevsen, P. D.: A conceptual model for glacial cycles and the middle Pleistocene transition, Climate Dynamics, 46, 29–40, 2016.

De Saedeleer, B., Crucifix, M., and Wieczorek, S.: Is the astronomical forcing a reliable and unique pacemaker for climate? a conceptual model study, Climate Dynamics, 40, 273–294, 2013.

Ditlevsen, P., Mitsui, T., and Crucifix, M.: Crossover and peaks in the Pleistocene climate spectrum; understanding from simple ice age models, Climate Dynamics, 54, 1801–1818, 2020.

Ditlevsen, P. D.: Extension of stochastic resonance in the dynamics of ice ages, Chemical Physics, 375, 403–409, https://doi.org/10.1016/j.chemphys.2010.05.022, http://dx.doi.org/10.1016/j.chemphys.2010.05.022, 2010.

Ditlevsen, P. D. and Ashwin, P. B.: Complex climate response to astronomical forcing: The middle-Pleistocene transition in glacial cycles and changes in frequency locking, Frontiers in Physics, 6, https://doi.org/10.3389/fphy.2018.00062, 2018.

Ditlevsen, P. D., Andersen, K. K., and Svensson, A.: The DO-climate events are probably noise induced: Statistical investigation of the claimed 1470 years cycle, Climate of the Past, 3, 129–134, https://doi.org/10.5194/cp-3-129-2007, 2007.

Drótos, G., Bódai, T., and Tél, T.: Probabilistic concepts in a changing climate: A snapshot attractor picture, Journal of Climate, 28, 3275–3288, 2015.

Duffing, G.: Erzwungene Schwingungen bei veränderlicher Eigenfrequenz und ihre technische Bedeutung, vol. 41/42 of *Sammlung Vieweg*, R. Vieweg & Sohn, Braunschweig, 1918.

Einstein, A.: Über die von der molekularkinetischen Theorie der Wärme geforderte Bewegung von in ruhenden Flüssigkeiten suspendierten Teilchen, Annalen der Physik, 322, 549–560; reprinted in *Investigations on the Theory of the Brownian Movement, five articles by A. Einstein*, R. Furth (ed.) and A. D. Cowper (transl.), 1956, Dover Publ., New York, 122 pp., 1905.

Emiliani, C. and Geiss, J.: On glaciations and their causes, Geologische Rundschau, 46, 576–601, 1959.

Fienga, A., Laskar, J., Exertier, P., Manche, H., and Gastineau, M.: Numerical estimation of the sensitivity of INPOP planetary ephemerides to general relativity parameters, Celestial Mechanics and Dynamical Astronomy, 123, 325–349, 2015.

FitzHugh, R.: Impulses and physiological states in theoretical models of nerve membrane, Biophysical journal, 1, 445–466, 1961.

Flint, R. F.: Glacial and Quaternary Geology, Wiley New York, 1971.

Ganopolski, A. and Brovkin, V.: Simulation of climate, ice sheets and CO2 evolution during the last four glacial cycles with an Earth system model of intermediate complexity, Climate of the Past, 13, 1695–1716, https://doi.org/10.5194/cp-13-1695-2017, 2017.

Ganopolski, A. and Calov, R.: The role of orbital forcing, carbon dioxide and regolith in 100 kyr glacial cycles, Climate of the Past, 7, 1415–1425, https://doi.org/10.5194/cp-7-1415-2011, 2011.

Ghil, M.: Climate stability for a Sellers-type model, Journal of the Atmospheric Sciences, 33, 3–20, 1976.

Ghil, M.: Climate sensitivity, energy balance models, and oscillatory climate models, Journal of Geophysical Research: Atmospheres, 89, 1280–1284, 1984.

Ghil, M.: Cryothermodynamics: the chaotic dynamics of paleoclimate, Physica D, 77, 130–159, 1994.

Ghil, M.: Hilbert problems for the geosciences in the 21st century, Nonlinear Processes in Geophysics, 8, 211–211, https://doi.org/10.5194/npg-8-211-2001, 2001.

Ghil, M.: Climate variability: Nonlinear and random aspects, in: Encyclopedia of Atmospheric Sciences, 2nd edn., edited by G. R. North, J. P. and Zhang, F., vol. 2, pp. 38–46, Elsevier, 2014.

Ghil, M.: A century of nonlinearity in the geosciences, Earth and Space Science, 6, 1007–1042, https://doi.org/10.1029/2019EA000599, 2019.

915 Ghil, M. and Childress, S.: Topics in Geophysical Fluid Dynamics: Atmospheric Dynamics, Dynamo Theory, and Climate Dynamics, Springer Science+Business Media, Berlin/Heidelberg, https://doi.org/10.1007/978-1-4612-1052-8, Reissued as an eBook in 2012, 978-1-4612-1052-8, 1987.

Ghil, M. and Le Treut, H.: A climate model with cryodynamics and geodynamics, Journal of Geophysical Research: Oceans, 86, 5262–5270, 1981.

920 Ghil, M. and Lucarini, V.: The physics of climate variability and climate change, Reviews of Modern Physics, 92, 035 002, https://doi.org/10.1103/RevModPhys.92.035002, 2020.

Ghil, M. and Tavantzis, J.: Global Hopf bifurcation in a simple climate model, SIAM Journal on Applied Mathematics, 43, 1019–1041, https://doi.org/10.1137/0143067, 1983.

Ghil, M. and Vautard, R.: Interdecadal oscillations and the warming trend in global temperature time series, Nature, 350, 324–327, 1991.

925 Ghil, M. and Zaliapin, I.: Understanding ENSO variability and its extrema: A delay differential equation approach, in: Extreme Events: Observations, Modeling and Economics, Geophysical Monograph 214, edited by Chavez, M., Ghil, M., and Urrutia-Fucugauchi, J., pp. 63–78, Wiley Online Library, 2015.

Ghil, M., Mullhaupt, A., and Pestiaux, P.: Deep water formation and Quaternary glaciations, Climate Dynamics, 2, 1–10, 1987.

Ghil, M., Chekroun, M. D., and Simonnet, E.: Climate dynamics and fluid mechanics: natural variability and related uncertainties, Physica
930 D: Nonlinear Phenomena, 237, 2111–2126, https://doi.org/10.1016/j.physd.2008.03.036, 2008.

Gildor, H. and Tziperman, E.: Sea ice as the glacial cycles' climate switch: Role of seasonal and orbital forcing, Paleoceanography, 15, 605–615, 2000.

Guckenheimer, J. and Holmes, P. J.: Nonlinear Oscillations, Dynamical Systems, and Bifurcations of Vector Fields, Applied Mathematical Sciences, Springer Science & Business Media, 1983.

935 Hasselmann, K.: Stochastic climate models. I: Theory, Tellus, 28, 473–485, 1976.

Hays, J. D., Imbrie, J., Shackleton, N. J., et al.: Variations in the Earth's orbit: pacemaker of the ice ages, science, 194, 1121–1132, 1976.

Heinrich, H.: Origin and consequences of cyclic ice rafting in the Northeast Atlantic Ocean during the past 130,000 years, Quaternary Research, 29, 142–152, https://doi.org/10.1016/0033-5894(88)90057-9, 1988.

Held, I. M.: The gap between simulation and understanding in climate modeling, Bulletin of the American Meteorological Society, 86,
940 1609–1614, https://doi.org/10.1175/bams-86-11-1609, 2005.

Held, I. M. and Suarez, M. J.: Simple albedo feedback models of the ice caps, Tellus, 26, 613–629, 1974.

Henry, L. G., McManus, J. F., Curry, W. B., Roberts, N. L., Piotrowski, A. M., and Keigwin, L. D.: North Atlantic ocean circulation and abrupt climate change during the last glaciation, Science, 353, 470–474, https://doi.org/10.1126/science.aaf5529, 2016.

Hoffman, P. F., Kaufman, A. J., Halverson, G. P., and Schrag, D. P.: A Neoproterozoic snowball earth, Science, 281, 1342–1346, 1998.

945 Hogg, A. M. C.: Glacial cycles and carbon dioxide: A conceptual model, Geophysical Research Letters, 35, 1–5, https://doi.org/10.1029/2007GL032071, 2008.

Huybers, P.: Glacial variability over the last two million years: an extended depth-derived agemodel, continuous obliquity pacing, and the Pleistocene progression, Quaternary Science Reviews, 26, 37–55, https://doi.org/10.1016/j.quascirev.2006.07.013, 2007.

Huybers, P.: Combined obliquity and precession pacing of late Pleistocene deglaciations, Nature, 480, 229–232,
950 https://doi.org/10.1038/nature10626, http://dx.doi.org/10.1038/nature10626, 2011.

Huybers, P. and Langmuir, C. H.: Delayed CO2 emissions from mid-ocean ridge volcanism as a possible cause of late-Pleistocene glacial cycles, Earth and Planetary Science Letters, 457, 238–249, 2017.

Huybers, P. J.: Pleistocene glacial variability as a chaotic response to obliquity forcing, Climate of the Past, 2009.

Imbrie, J. and Imbrie, J. Z.: Modeling the Climatic Response to Orbital Variations, Science, 207, 943–953, 1980.

Imbrie, J. and Imbrie, K. P.: Ice Ages: Solving the Mystery, 2nd ed., Harvard University Press, 1986.

Imbrie, J. Z., Imbrie-Moore, A., and Lisiecki, L. E.: A phase-space model for Pleistocene ice volume, Earth and Planetary Science Letters, 307, 94–102, https://doi.org/10.1016/j.epsl.2011.04.018, http://dx.doi.org/10.1016/j.epsl.2011.04.018, 2011.

Isaacson, E. and Keller, H. B.: Analysis of numerical methods, Dover Publications, Inc., New York, NY, 2012.

Jackson, E. A.: Perspectives of Nonlinear Dynamics, Cambridge University Press, New York, 1991.

Jordan, D. W. and Smith, P.: Nonlinear Ordinary Differential Equations – An Introduction for Scientists and Engineers, Oxford University Press, Oxford/New York, 2 edn., 1987.

Källén, E., Crafoord, C., and Ghil, M.: Free oscillations in a climate model with ice-sheet dynamics, Journal of the Atmospheric Sciences, 36, 2292–2303, 1979.

Kwasniok, F.: Analysis and modelling of glacial climate transitions using simple dynamical systems, Philosophical Transactions of the Royal Society A: Mathematical, Physical and Engineering Sciences, 371, https://doi.org/10.1098/rsta.2011.0472, 2013.

Landau, L. D. and Lifshitz, E. M.: Mechanics, vol. I of Course on Theoretical Physics, Pergamon Press, Oxford, 1960.

Laskar, J., Robutel, P., Joutel, F., Gastineau, M., Correia, A., and Levrard, B.: A long-term numerical solution for the insolation quantities of the Earth, Astronomy & Astrophysics, 428, 261–285, 2004.

Le Treut, H. and Ghil, M.: Orbital forcing, climatic interactions, and glaciation cycles, Journal of Geophysical Research: Oceans, 88, 5167–5190, 1983.

Le Treut, H., Portes, J., Jouzel, J., and Ghil, M.: Isotopic modeling of climatic oscillations: Implications for a comparative study of marine and ice core records, Journal of Geophysical Research: Atmospheres, 93, 9365–9383, 1988.

Lenssen, N. J. L., Schmidt, G. A., Hansen, J. E., Menne, M. J., Persin, A., Ruedy, R., and Zyss, D.: Improvements in the GISTEMP uncertainty model, Journal of Geophysical Research: Atmospheres, 124, 6307–6326, 2019.

Lisiecki, L. E. and Raymo, M. E.: A Pliocene-Pleistocene stack of 57 globally distributed benthic δ18O records, Paleoceanography, 20, 2005.

Lorenz, E. N.: Deterministic nonperiodic flow, Journal of the Atmospheric Sciences, 20, 130–141, 1963.

Maasch, K. A. and Saltzman, B.: A Low-Order Dynamical Model of Global Climatic Variability Over the Full Pleistocene, Journal of Geophysical Research, 95, 1955–1963, 1990.

Marangio, L., Sedro, J., Galatolo, S., Di Garbo, A., and Ghil, M.: Arnold maps with noise: Differentiability and non-monotonicity of the rotation number, Journal of Statistical Physics, 179, 1–31, https://doi.org/10.1007/s10955-019-02421-1, 2019.

Matteucci, G.: Orbital forcing in a stochastic resonance model of the Late-Pleistocene climatic variations, Climate Dynamics, 3, 179–190, https://doi.org/https://doi.org/10.1007/BF01058234, 1989.

Milankovitch, M.: Théorie mathématique des phénomènes thermiques produits par la radiation solaire, Gauthier-Villars, Paris, 1920.

Mitsui, T. and Aihara, K.: Dynamics between order and chaos in conceptual models of glacial cycles, Climate Dynamics, 42, 3087–3099, https://doi.org/10.1007/s00382-013-1793-x, 2014.

Mitsui, T. and Crucifix, M.: Influence of external forcings on abrupt millennial-scale climate changes: a statistical modelling study, Climate Dynamics, 48, 2729–2749, 2017.

Mitsui, T., Crucifix, M., and Aihara, K.: Bifurcations and strange nonchaotic attractors in a phase oscillator model of glacial–interglacial cycles, Physica D: Nonlinear Phenomena, 306, 25–33, 2015.

990 Nagumo, J., Arimoto, S., and Yoshizawa, S.: An active pulse transmission line simulating nerve axon, Proceedings of the IRE, 50, 2061–2070, 1962.

National Research Council: Understanding Climatic Change, a Program for Action, National Academy of Sciences, Washington, DC, 239 pages, 1975.

Nicolis, C.: Solar variability and stochastic effects on climate, Solar Physics, 74, 473–478, https://doi.org/10.1007/BF00154530, 1981.

995 Nicolis, G. and Nicolis, C.: Foundations of Complex Systems, World Scientific, 2nd edn., https://doi.org/10.1142/8260, https://www.worldscientific.com/doi/abs/10.1142/8260, 2012.

North, G. R.: Analytical solution to a simple climate model with diffusive heat transport, Journal of the Atmospheric Sciences, 32, 1301–1307, 1975.

North Greenland Ice Core Project members: High-resolution record of the Northern Hemisphere climate extending into the last interglacial
1000 period, Nature, 431, 147–151, 2004.

Oerlemans, J.: Model experiments on the 100,000-yr glacial cycle, Nature, 287, 430–432, 1980.

Oerlemans, J.: On the origin of the ice ages, in: Milankovitch and Climate: Understanding the Response to Astronomical Forcing, vols. I & II, edited by Berger, A., Imbrie, J., Hays, J., Kukla, G., and Saltzman, B., pp. 607–611, D. Reidel Publ. Co., 1984.

Omta, A. W., Kooi, B. W., van Voorn, G. A., Rickaby, R. E., and Follows, M. J.: Inherent characteristics of sawtooth cycles can explain
1005 different glacial periodicities, Climate dynamics, 46, 557–569, 2016.

Paillard, D.: The timing of Pleistocene glaciations from a simple multiple-state climate model, Nature, 391, 378–381, 1998.

Paillard, D.: Glacial cycles: Toward a new paradigm, Reviews of Geophysics, 39, 325–346, https://doi.org/https://doi.org/10.1029/2000RG000091, 2001.

Paillard, D. and Parrenin, F.: The Antarctic ice sheet and the triggering of deglaciations, Earth and Planetary Science Letters, 227, 263–271,
1010 https://doi.org/10.1016/j.epsl.2004.08.023, 2004.

Parrenin, F. and Paillard, D.: Amplitude and phase of glacial cycles from a conceptual model, Earth and Planetary Science Letters, 214, 243–250, https://doi.org/10.1016/S0012-821X(03)00363-7, 2003.

Parrenin, F. and Paillard, D.: Terminations VI and VIII ($\sim$ 530 and $\sim$ 720 kyr BP) tell us the importance of obliquity and precession in the triggering of deglaciations, Climate of the Past, 8, 2031–2037, https://doi.org/10.5194/cp-8-2031-2012, 2012.

1015 Pelletier, J. D.: Coherence resonance and ice ages, Journal of Geophysical Research, 108, 1–14, https://doi.org/10.1029/2002jd003120, 2003.

Pierini, S. and Ghil, M.: Climate tipping points induced by parameter drift: an excitable system study, Scientific Reports, in press, 2021.

Pierini, S., Ghil, M., and Chekroun, M. D.: Exploring the pullback attractors of a low-order quasigeostrophic ocean model: The deterministic case, Journal of Climate, 29, 4185–4202, 2016.

Pierini, S., Chekroun, M. D., and Ghil, M.: The onset of chaos in nonautonomous dissipative dynamical systems: A low-order ocean–model
1020 case study, Nonlin. Processes Geophys., 25, 671–692, https://doi.org/10.5194/npg-25-671-2018, 2018.

Pierrehumbert, R. T.: High levels of atmospheric carbon dioxide necessary for the termination of global glaciation, Nature, 429, 646–649, https://doi.org/10.1038/nature02640, 2004.

Pikovsky, A., Rosenblum, M. G., and Kurths, J.: Synchronization, A Universal Concept in Nonlinear Sciences, Cambridge University Press, Cambridge, 2001.

1025 Pikovsky, A. S. and Kurths, J.: Coherence resonance in a noise-driven excitable system, Physical Review Letters, 78, 775–778, https://doi.org/10.1103/physrevlett.78.775, 1997.

Poincaré, H.: Méthodes nouvelles de la Mécanique céleste, vols. I-III, Gauthier-Villars, 1892–1899.

Pollard, D.: A coupled climate-ice sheet model applied to the Quaternary ice ages, Journal of Geophysical Research: Oceans, 88, 7705–7718, 1983.

1030   Quinn, C., Sieber, J., Von Der Heydt, A. S., and Lenton, T. M.: The Mid-Pleistocene Transition induced by delayed feedback and bistability, arXiv, pp. 1–17, https://doi.org/10.1093/climsys/dzy005, 2017.

Rasmussen, S. O., Bigler, M., Blockley, S. P., Blunier, T., Buchardt, S. L., Clausen, H. B., Cvijanovic, I., Dahl-Jensen, D., Johnsen, S. J., Fischer, H., et al.: A stratigraphic framework for abrupt climatic changes during the Last Glacial period based on three synchronized Greenland ice-core records: refining and extending the INTIMATE event stratigraphy, Quaternary Science Reviews, 106, 14–28, 2014.

1035   Rial, J. A. and Yang, M.: Is the frequency of abrupt climate change modulated by the orbital insolation?, Geophysical Monograph Series, 173, 167–174, https://doi.org/10.1029/173GM12, 2007.

Roberts, A. and Saha, R.: Relaxation oscillations in an idealized ocean circulation model, Climate Dynamics, 48, 2123–2134, https://doi.org/10.1007/s00382-016-3195-3, 2017.

Rocsoreanu, C., Georgescu, A., and Giurgiteanu, N.: The FitzHugh-Nagumo model: bifurcation and dynamics, vol. 10, Springer Science &
1040   Business Media, 2012.

Rousseau, D.-D., Antoine, P., Boers, N., Lagroix, F., Ghil, M., Lomax, J., Fuchs, M., Debret, M., Hatté, C., Moine, O., Gauthier, C., Jordanova, D., and Jordanova, N.: Dansgaard-Oeschger–like events of the penultimate climate cycle: the loess point of view, Climate of the Past, 16, 713–727, https://doi.org/10.5194/cp-16-713-2020, 2020.

Rousseau, D.-D., Bagniewski, W., and Ghil, M.: Abrupt climate changes and the astronomical theory: are they related?, Climate of the Past,
1045   18, 249–271, https://doi.org/10.5194/cp-18-249-2022, 2022.

Ruddiman, W. F. and McIntyre, A.: The North Atlantic Ocean during the last deglaciation, Palaeogeography, Palaeoclimatology, Palaeoecology, 35, 145–214, 1981.

Rulkov, N. F., Sushchik, M. M., Tsimring, L. S., and Abarbanel, H. D. I.: Generalized synchronization of chaos in directionally coupled chaotic systems, Physical Review E, 51, 980–994, https://doi.org/10.1103/physreve.51.980, 1995.

1050   Saltzman, B. and Maasch, K. A.: Carbon cycle instability as a cause of the late Pleistocene ice age oscillations: modeling the asymmetric response, Global Biogeochemical Cycles, 2, 177–185, 1988.

Saltzman, B. and Maasch, K. A.: A first-order global model of late Cenozoic climatic change, Transactions of the Royal Society of Edinburgh: Earth Sciences, 81, 315–325, https://doi.org/10.1017/S0263593300020824, 1990.

Saltzman, B. and Maasch, K. A.: A first-order global model of late Cenozoic climatic change II. Further analysis based on a simplification
1055   of CO2 dynamics, Climate Dynamics, 5, 201–210, https://doi.org/10.1007/BF00210005, 1991.

Saltzman, B. and Sutera, A.: The mid-Quaternary climatic transition as the free response of a three-variable dynamical model, Journal of the Atmospheric Sciences, 44, 236–241, 1987.

Saltzman, B., Sutera, A., and Evenson, A.: Structural stochastic stability of a simple auto-oscillatory climatic feedback system, Journal of the Atmospheric Sciences, 38, 494–503, 1981.

1060   Schneider, S. H. and Dickinson, R. E.: Climate modelling, Reviews of Geophysics and Space Physics, 25, 447–493, 1974.

Seierstad, I. K., Abbott, P. M., Bigler, M., Blunier, T., Bourne, A. J., Brook, E., Buchardt, S. L., Buizert, C., Clausen, H. B., Cook, E., Dahl-Jensen, D., Davies, S. M., Guillevic, M., Johnsen, S. J., Pedersen, D. S., Popp, T. J., Rasmussen, S. O., Severinghaus, J. P., Svensson, A., and Vinther, B. M.: Consistently dated records from the Greenland GRIP, GISP2 and NGRIP ice cores for the past 104 ka reveal regional millennial-scale δ18O gradients with possible Heinrich event imprint, Quaternary Science
1065   Reviews, 106, 29–46, https://doi.org/https://doi.org/10.1016/j.quascirev.2014.10.032, https://www.sciencedirect.com/science/article/pii/

S027737911400434X, dating, Synthesis, and Interpretation of Palaeoclimatic Records and Model-data Integration: Advances of the IN-TIMATE project(INTegration of Ice core, Marine and TErrestrial records, COST Action ES0907), 2014.

Sellers, W. D.: A global climatic model based on the energy balance of the Earth atmosphere, Journal of Applied Meteorology, 8, 392–400, 1969.

Sergin, V. Y.: Numerical modeling of the glaciers-ocean-atmosphere global system, Journal of Geophysical Research: Oceans, 84, 3191–3204, 1979.

SMIC: Inadvertent Climate Modification: Report of the Study of Man's Impact on Climate, The MIT Press, Cambridge, Mass., 308 pp., 1971.

Talento, S. and Ganopolski, A.: Reduced-complexity model for the impact of anthropogenic CO_2 emissions on future glacial cycles, Earth System Dynamics, 12, 1275–1293, https://doi.org/10.5194/esd-12-1275-2021, 2021.

Toggweiler, J.: Origin of the 100,000-year timescale in Antarctic temperatures and atmospheric CO_2, Paleoceanography, 23, 2008.

Tziperman, E. and Gildor, H.: The stabilization of the thermohaline circulation by the temperature–precipitation feedback, Journal of Physical Oceanography, 32, 2707–2714, 2002.

Tziperman, E., Raymo, M. E., Huybers, P., and Wunsch, C.: Consequences of pacing the Pleistocene 100 kyr ice ages by nonlinear phase locking to Milankovitch forcing, Paleoceanography, 21, 1–11, https://doi.org/10.1029/2005PA001241, 2006.

Van der Pol, B.: On relaxation-oscillations, The London, Edinburgh and Dublin Phil. Mag. and J. Sci., 2, 978–992, 1926.

Vannitsem, S., Demaeyer, J., and Ghil, M.: Extratropical low-frequency variability with ENSO forcing: A reduced-order coupled model study, J. Adv. Model. Earth Syst., p. e2021MS002530, 2021.

Varadi, F., Runnegar, B., and Ghil, M.: Successive refinements in long-term integrations of planetary orbits, The Astrophysical Journal, 592, 620–630, 2003.

Verbitsky, M. Y. and Crucifix, M.: π-theorem generalization of the ice-age theory, Earth System Dynamics, 11, 281–289, 2020.

Verbitsky, M. Y., Crucifix, M., and Volobuev, D. M.: A theory of Pleistocene glacial rhythmicity, Earth System Dynamics, 9, 1025–1043, https://doi.org/10.5194/esd-9-1025-2018, 2018.

Vettoretti, G., Ditlevsen, P., Jochum, M., and Rasmussen, S. O.: Millennial-scale Ice Age Climate Oscillations Controlled by Atmospheric CO_2, Nature Geoscience, under review.

Vissio, G., Lembo, V., Lucarini, V., and Ghil, M.: Evaluating the performance of climate models based on Wasserstein distance, Geophysical Research Letters, 47, e2020GL089 385, https://doi.org/10.1029/2020GL089385, 2020.

Wang, B.: Random attractors for the stochastic FitzHugh-Nagumo system on unbounded domains, Nonlinear Analysis, Theory, Methods and Applications, 71, 2811–2828, https://doi.org/10.1016/j.na.2009.01.131, 2009.

Weertman, J.: Rate of growth or shrinkage of non-equilibrium ice-sheets, J. Glaciology, 6, 145–158, 1964.

Weertman, J.: Milankovitch solar radiation variations and ice-age ice-sheet sizes, Nature, 261, 17–20, 1976.

Westerhold, T., Marwan, N., Drury, A. J., Liebrand, D., Agnini, C., Anagnostou, E., Barnet, J. S. K., Bohaty, S. M., De Vleeschouwer, D., Florindo, F., et al.: An astronomically dated record of Earth's climate and its predictability over the last 66 million years, Science, 369, 1383–1387, 2020.

Wetherald, R. T. and Manabe, S.: The effects of changing the solar constant on the climate of a general circulation model, Journal of the Atmospheric Sciences, 32, 2044–2059, 1975.

Wilkinson, L. and Friendly, M.: The History of the Cluster Heat Map, The American Statistician, 63, 179–184, https://doi.org/10.1198/tas.2009.0033, 2009.

Willeit, M., Ganopolski, A., Calov, R., and Brovkin, V.: Mid-Pleistocene transition in glacial cycles explained by declining CO2 and regolith removal, Science Advances, 5, eaav7337, 2019.

Yamakou, M. E., Tran, T. D., Duc, L. H., and Jost, J.: The stochastic Fitzhugh–Nagumo neuron model in the excitable regime embeds a leaky integrate-and-fire model, Journal of Mathematical Biology, 79, 509–532, https://doi.org/10.1007/s00285-019-01366-z, 2019.

Zhang, G., Liu, Z., and Ma, Z.: Generalized synchronization of different dimensional chaotic dynamical systems, Chaos, Solitons & Fractals, 32, 773–779, https://doi.org/10.1016/j.chaos.2005.11.099, 2007.